Chapter 10

Zinc Oxide Nanoparticles and Photodynamic Therapy for the Treatment of B-chronic Lymphocytic Leukemia

Sandra Loydover Peña Luengas, Gustavo H. Marin, Luis Rivera, Adrian Tarditti, Gustavo Roque and Eduardo Mansilla

Additional information is available at the end of the chapter

http://dx.doi.org/10.5772/61796

Abstract

The generation of singlet oxygen (SO) in the presence of specific photosensitizers (PS) or semiconductor nanoparticles (NPs) and its application in photodynamic therapy (PDT) has great interest for the development of new cancer therapies. Our work focused on the identification of factors leading to the enhancement of B-Chronic Lymphocytic Leukemia (B-CLL) intracellular SO production and cell killing using Manganese (Mn) doped and undoped Zinc Oxide (ZnO) NPs as potential photosensitizers with and without PDT. Mn can enhance ZnO NPs generation of SO by targeted cells. Multi drug resistant B-Chronic Lymphocytic Leukemia (B-CLL) cells spontaneously produce high amounts of Reactive Oxygen Species (ROS) having an altered redox state in relation to that of normal B lymphocytes. These little variations of its SO intracellular concentrations could allow ZnO NPs to execute specific deadly programs against these leukemic cells with no significant damage to normal lymphocytes. A 0.5% Mn Doped ZnO NP was finally selected for further probes as it had the best killing activity in fludarabine resistant B-CLL cells, especially when combined with PDT. This could be an innovative specific therapy against resistant B-CLL probably contributing in the near future for the definitive benefit of these bad prognostic patients.

Keywords: ZnO, Naoparticles, PDT, Leukemia

1. Introduction

B-chronic lymphocytic leukemia (B-CLL) and other chronic indolent hematologic malignancies like B lymphomas are diseases that usually originate from hematopoietic B cells with abnormal alterations in the processes of development, maturation, and/or apoptosis. They usually manifest as progressive accumulations of morphologically mature B lymphocytes

although immunologically dysfunctional [1, 2]. B-CLL is the most common adult leukemia in the western world, and currently it has no available curative strategy [1]. Beside many new discoveries for its treatment, advanced stages of B-CLL usually derived in drug resistance and aggressive progression with the death of the majority of patients [3, 4]. Chemotherapy is still a valid alternative for its temporary improvement or just for tumor mass reduction but not for a definitive healing treatment modality as it has been said [3]. The gold standard of any antineoplastic drug should be to submit the malignant cells to an apoptotic or cytotoxic program, without involving healthy ones, thereby minimizing adverse effects and maximizing the expected results, especially in those situations where drug resistance has developed [5, 6, 7]. Therefore, it is essential to have new treatment modalities in order to increase the anti-B-CLL effects, providing greater biological activity and much more specificity for this kind of disease. New drugs as well as monoclonal antibodies and other biologics have shown real improvements as antineoplastic therapies [8, 9]. However, in general, the side effects are also frequent, and the development of resistance or relapse is usually inevitable for these kind of diseases [3, 5, 10, 11]. In order to minimize adverse effects, new drug delivery strategies should be designed for therapeutic or diagnostic purposes in oncology. Thus, when such an agent is desired to be specifically delivered inside a tumor mass, innovations are needed. In our present state of knowledge, the systemic administration of antineoplastic drugs usually faces problems related to nondesired effects in healthy tissues and incomplete distribution inside the targeted tumor [12]. Then "specific targeted therapies" (STT) could be the new hope for solid and hematological tumors [13]. Advancements in materials science and the ever-increasing miniaturization of technology have led to the development of nanotechnology, a discipline concerned with the development and utilization of nanomaterials, structures with dimensions in the 1- to 100-nm range [14, 15, 16]. Nanoparticles (NPs) are increasingly being recognized for their utility in the field of medicine, including use as drug carriers and imaging tools [17, 18, 19]. Investigations of reactive species (free atoms, clusters, and reactive particles) throughout the 1970s and 1980s, coupled with new techniques and instruments (innovations in mass spectrometry, vacuum technology, microscopes, and more), brought nanotechnology to different fields, including chemistry, physics, material science, engineering, and biology [20]. Today, nanoscale materials represent real and widespread possibilities for interesting fundamental science as well as useful technologies [21, 22]. Nanotechnology and nanoscience are multidisciplinary fields between chemistry, which deals with atoms, molecules, and condensed matter physics, which deals with solids of an essentially infinite array of bound atoms or molecules of dimension no greater than 100 nm [23]. We have now the unique opportunity to change some properties of materials through the management of size and shape. This is a central point of nanoscience that will permit us the control of some electronic as well as magnetic conditions of matter by which it can become much more active and useful for cancer treatments [24, 25, 26, 27, 28, 29]. Although the 8 physical and chemical properties of substances have been well characterized, an intriguing facet of nanotechnology is that materials reduced to the nanoscale in size begin to display different physical and chemical properties. This can include changes in optical properties, such as color and light diffraction, solubility, hardness and strength, magnetism, heat, and electrical conductivity, and surface reactivity [21, 30]. As NP size is reduced, the surface area-to-volume ratio increases, and a large number of the atoms

http://dx.doi.org/10.5772/61796

composing the particle are found on the particle surface [31]. This can render substances previously thought inert suddenly highly reactive. These changes in properties mean that researchers cannot rely upon expectations of chemical behavior based on the previously understood characteristics of these substances [20, 32]. In NPs made of semiconducting materials, the band gap can be modified with NP size [33, 34, 35]. The band gap is the amount of energy required for an electron in the material to be liberated from the allowed valence band and become a charge carrier. If enough energy is supplied, an electron jumps from the valence band to the conductance band, leaving behind a vacancy called an electron hole in the valance band. In NPs, a large portion of the atoms are found at the surface, and consequently so too are the highly reactive valence electrons and holes. This has strong implications for the potential of NP to have toxic reactivity in biological systems [36, 37, 38, 39]. The formation of vesicles or capsules that are small enough to be delivered into the human body by means of inhalation, injection, or permeation through the skin has received significant attention [40]. The outer shell of the vesicles may be chemically functionalized with receptors and other species to selectively target certain organs [41]. In this way, it is possible to think between some other strategies, in the use of delivery/antineoplastic systems that could be delivered easily straight into the tumor's cells. By using nanoparticle systems, it is possible now to provide more precisely many drugs and peptides specifically inside the tumors [7, 42, 43]. These nanoparticles can be made of biodegradable as well as nonbiodegradable materials. Some of their effects could be derived from its abilities to transport and deliver drugs, reducing toxicity as well as increasing bioavailability or even by a direct effect of their molecular and electrical properties as it is the case for some metallic nanoparticles [8, 44]. When they are designed to transport drugs, it is clear that they can specifically deliver them in huge amounts and very specifically inside neoplastic cells without much harm to healthy ones [9, 45]. This has been described for cisplatin in which a higher apoptosis process was observed than with a free drug [10]. These nanopharmaceuticals as multifunctional drugs and imaging agents with a very wide repertoire of action will surely be the next generation of antineoplastic therapeutic and diagnostic agents [11, 46]. There is some previous but limited published experience with NPs in lymphomas, including in vivo studies in lymphoproliferative diseases [42–44]. We have already published [47] the possibility of using these pharmaceutical new systems to overcome drug resistance of B-chronic lymphocytic leukemia (B-CLL) cells. Nanotechnology, the science that studies, develops, and employs nanometer-scale complex systems, has claimed to be the key to improve treatment outcomes in oncology [33, 48, 49]. Then NPs, objects of a size of tens to hundreds of nanometers as it has been said, constructed with different materials such as natural or synthetic polymers or even metals, could be custom designed for almost every disease, including B-CLL and other lymphomas [47, 50]. These elements when made of zinc oxide (ZnO) are plausible to be coated and modified by other metals like manganese (Mn) and could generate apoptotic and/or cytotoxic changes in malignant cells, especially in the shape of autophagy. This specialized way of tumor cell death seems to be the specific result of metal NPs action and could be an interesting and innovative mechanism to be full discovered and achieved in cancer treatment [51, 52]. ZnO NPs doped with metals such as Mn may have their optical and electronic properties modified as Mn is known to increase metal NP's surface defects, thus generating photooxidation reactions that could be enhanced by PDT [53, 54, 55].

In this way, we thought that these NPs made of Mn-doped ZnO could be used in the treatment of B-CLL and other indolent lymphomas, alone or in combination with PDT. These NPs, by itself or even more if excited by light emission, may generate ROS especially one of its kind, singlet oxygen (SO), which could lead to an induced apoptotic process or some other kind of death pathway like autophagy in B-CLL cells, including those with resistant phenotypes to conventional therapies [56, 57]. This strategy could be a very specific one, considering that the oxidative stress found in leukemic cells is supposed to be a lot much higher than that of normal B lymphocytes [6, 7]. Based on a growing body of evidence, ROS production is proposed as a key cytotoxic mechanism mediated by ZnO NPs leading to cell death [58, 59]. The photoactivation of these ZnO NPs is predicted to induce greater levels of ROS, including intracellular SO release which, if effectively targeted to cancer cells, could produce their selective final destruction [48, 60]. The use of ZnO nanoparticles (NPs) for biomedical applications, particularly PDT, relies on the fact that semiconductor nanomaterials could generate reactive oxygen species (ROS) and are promising candidates to become the new generation of photosensitizers (PS) [61]. ZnO is an excellent PS candidate due to its nontoxicity and ability to biodegrade [62, 63]. Moreover, it displays high thermal and chemical stabilities [64]. Furthermore, ZnO is a high-quality semiconductor material with a band gap of 3.37 eV, is transparent in the UV region, and has a large excitation binding energy at room temperature (60 meV) [65]. ZnO has the hexagonal wurtzite structure with lattice parameters a = 3.29Å and c = 5.24 Å) [65]. Cancer disease has been one of the principal causes of death worldwide for many years [66, 67]. Photodynamic therapy (PDT) has been successful in the treatment of skin tumors and superficial skin health conditions [68, 69, 70]. We propose to expand the applicability of PDT for therapeutic purposes on other cancer types, which involve internal organs, including the hematological system, and in this respect, NPs possess various physical characteristics, which make them ideal for cancer targeting and treatment using them as PS with PDT [48, 71]. Some of these physical characteristics are size in the nanometer scale for cell membrane internalization, intense emission for illumination, and stability. In addition, they can be prepared with absorption at definite wavelengths to tune them to penetrate into deep seated tumors. Nanotechnology, in fact, has recently been utilized for specific targeting to tumor cells [60, 71] as opposed to current technology based on drug diffusion upon systemic drug uptake, which only reaches a maximum of 30% to the intended site and with the added secondary harmful effects on health. In PDT, a nanoparticle sensitizer is excited at its maximum absorption wavelength, thereby being promoted to its singlet excited state, which then is converted into its triplet state by intersystem crossing [72, 73]. Then the triplet state of the NP transfers energy to the ground state triplet oxygen, which is converted to singlet oxygen (SO) [74, 75]. The search for efficient sensitizers for in situ SO generation is currently of utmost importance for use in PDT [73, 74]. Diverse organic molecules have been synthesized, incorporating different structural features that have been identified with enhanced SO production. NPs have recently been identified as potential sensitizer candidates for SO generation due to their high extinction coefficients, and a few reports have been published [48, 71]. We proposed to use nontoxic functionalized water-soluble ZO and zinc sulfide (ZS) NPs as enhanced SO photosensitizers and to identify factors for their enhanced SO production for improved cancer treatment especially for B-CLL.

http://dx.doi.org/10.5772/61796

2. PDT and metal NPs for cancer treatment

Photodynamic therapy (PDT) is a form of phototherapy using nontoxic light-sensitive compounds that are exposed selectively to light, whereupon they become toxic to targeted malignant and other diseased cells [21, 22]. It is used clinically to treat a wide range of medical conditions, including wet age-related macular degeneration and malignant cancers [23] and is recognized as a treatment strategy, which is both minimally invasive and minimally toxic. Most modern PDT applications involve three key components: [21] a photosensitizer, a light source, and tissue oxygen. The combination of these three components leads to the chemical destruction of any tissues, which either have selectively taken up the photosensitizer or have been locally exposed to light [22]. The wavelength of the light source needs to be appropriate for exciting the photosensitizer to produce ROS [22]. These ROS generated through PDT are free radicals (Type I PDT) generated through electron abstraction or transfer from a substrate molecule and highly reactive state of oxygen known as SO (Type II PDT) [22, 70]. A photosensitizer is a chemical compound that can be promoted to an excited state upon absorption light and undergo intersystem crossing with oxygen to produce SO. The photosensitizer should not be harmful to the target tissue until the treatment beam is applied and preferential uptake in target tissue. Some of these physical characteristics are size in the nanometer scale for cell membrane internalization as well as intense emission for illumination and stability [21, 22]. In PDT, a nanoparticle sensitizer is excited at its maximum absorption wavelength, thereby being promoted to its singlet excited state, which then is converted into its triplet state [23]. Then the triplet state of the nanoparticle transfers energy to the ground state triplet oxygen, which is converted to singlet oxygen (SO) [22]. Metal oxides (MO) play a very important role in many areas of chemistry, physics, and materials science. MO NPs can exhibit unique physical and chemical properties due to their limited size and a high density of corner or edge surface sites [23]. MO NPs include materials such as TiO_2, CeO_2, Al_2O_3, Fe_2O_3, and ZnO and are already found in many products. TiO_2 and ZnO nanomaterials are used in topically applied products such as sunscreens and cosmetics, as are pure gold NPs [76]. Their remarkable physical properties form the basis for motivation of metal NPs synthesis and large effort has especially been focused on the design, characterization, and medical applications of ZnO nanomaterials [77]. Inorganic semiconductor nanocrystals have unique properties resulting from quantum confinement [78]. For semiconductor nanocrystals, the energy gap increases with decreasing size [79]. The excitation tracks the absorbance, resulting in a tunable fluorophore that can be excited efficiently at any wavelength shorter than the emission peak but will emit with the same characteristic narrow, symmetric spectrum regardless of the excitation wavelength [80]. ZnO, also known as zincite, is an inorganic compound, nearly insoluble in water that occurs rarely in nature. It is mostly produced synthetically for its commercial used [65,81]. ZnO is actually a wideband gap semiconductor of the II–VI semiconductor group [76]. At a nanoscale, size exhibits quantum confinement as its electrons are contained in discrete energy bands. In this way and when sufficient energy is supplied, electrons can move from the valence to the conductance band, being able to act as powerful reductants in aqueous solutions as well as mobile charge carriers donating electrons to oxygen to generate superoxide radicals [81, 82]. When this electron movement into the conductance band occurs, there are electron vacancies that can produce powerful oxidation reactions in water. This production of hydrogen peroxide and photocatalysis of ROS by NP-sized ZnO in water can be 100–1000 times faster than bulk ZnO [83, 84].

2.1. Methodology and experimental procedures

2.1.1. Synthesis of NPs

Eight different types of Zn NPs were synthesized by different methods as described here: NP1 ZnO, NP2 ZnO:Mn^{+2} 0.5%, NP3 ZnO:Mn^{+2} 1.0%, NP4 ZnO:Mn^{+2} 1.5%, NP5 ZnO:Mn^{+2} 2.0%, NP6 ZnS, NP7 ZnS:Mn^{+2} 1.0%, and NP8 ZnO/ZnS. NPs were finally diluted and prepared for all experiments by vigorous sonication and addition of human serum albumin.

a. Synthesis of ZnO and Mn-doped ZnO NPs: These NPs were synthesized via wet-chemical techniques [53, 85]. The different Mn doping percentages applied on the surface of NPs were 0.5%, 1.0%, 1.5%, and 2.0%. Undoped ZnO NPs were synthesized with a similar procedure except for the addition of manganese acetate [53].

b. Synthesis of colloidal ZnS semiconductor nanocrystals capped with PVP and prepared using 1% concentration of Mn^{+2} ion as a dopant: The NPs were synthesized via wet-chemical techniques [86]. Undoped ZnS NPs were synthesized with a similar procedure except for the addition of manganese acetate [87].

c. Synthesis of ZnO/ZnS core shell NPs: The preparation of ZnO/ZnS core shell NPs was performed by the thermal decomposition of Zn-MPA complexes [88, 89]. ZnS shell was grown on ZnO nanoparticle by the decomposition of the complex Zn-MPA(3-mercapto-propionic acid) at 100°C. The S atoms originating from the thermal decomposition are deposited slowly.

2.1.2. Characterization of NPs

We characterized all NPs by transmission electron microscopy (TEM) (JEM-2100F, JEOL Inc.) and scanning electron microcopy (SEM) (JEOL-JSM 6500 instrument and a Philips/FEI, XL30s, FEG SEM/Phoenix EDAX) observation after the deagglomeration of NPs with human serum albumin (HSA) 1.5 mg/mL and intense sonication, as well as by elemental composition analysis by energy-dispersive X-ray spectroscopy (EDS). Also, X-ray diffraction (XRD) measurements were carried out with a diffractometer (D500/Siemens) using Cu-Kα radiation with $\lambda = 0.154315$ nm to determine the crystalline nature of the selected NPs. A UV-Vis spectrophotometer (DU 800, Beckman Coulter) was used to study the optical absorption of NPs. Luminescence properties and SO generation by NPs were determined by photoluminescence (PL) spectroscopy, using a spectrofluorometer (FluoroMax-2/Horiba Scientific) at room temperature with a 150-mW continuous ozone-free Xe lamp. Fourier-transformed infrared (FTIR) spectra was recorded using an attenuated total reflection Fourier transform infrared (FTIR-Varian 3100 FTIR/Bio-Rad) to evaluate and characterized the presence of functional groups on the surface of these NPs. The excitation wavelength for photoluminescence measurements was set at 350 nm for ZnO and manganese-doped ZnO NPs, and the excitation wavelengths for ZnS NPs were 320 and 340 nm for manganese-doped ZnS NPs. The excitation wavelength for ZnO/ZnS core shell nanoparticles was 310 nm. For book space reasons, we will only describe here the characterization in full detail only of that type of NP with the best B-CLL cytotoxic effects when applying PDT and tested in vitro for viability and mortality of leukemic cells as later will be described.

http://dx.doi.org/10.5772/61796

2.1.3. Penetration of cells by NPs

Amounts of 0.1, 0.2, and 0.3 mg/mL of each of the eight NPs produced were incubated with 4 million cells in 2 mL of culture medium for a maximum period of 3 h, under conditions already described. NP penetration of cells was determined by TEM and by fluorescence microscopy (Motic Inverted Microscope AE30-31 with Episcopic-Fluorescence Attachment EF-INV-II) using a DAPI filter. The degree of penetration was determined by 3 independent pathologists observers trained in cell observation with TEM by evaluation of 5 pictures taken at every each time point (0, 30, 60, 120, and 180 min) of incubation of the cells with the different NPs and its selected concentrations mentioned before. For this purpose, cells with NPs were submitted to two washing cycles and finally to a resuspension step in PBS before TEM observation was performed. Results were the mean of the penetration scores given by all the observers to the 5 pictures for each specific NP and its different concentrations at every time point. Finally, the level of penetration was ranked in relation of the total cell surface covered with NPs as none (0–5%), discrete (6–45%), moderate (46–75%), or intense (76–100%), as seen in each TEM picture by each observer. The time at which the highest level of cell penetration by NPs occurred was later used as the best time point for all laser irradiation experiments. When maximum NP penetration of cells was determined by TEM, the confirmation of these data was done by observation of cells under fluorescence microscopy using a DAPI filter in which the cells were supposed to fluorescence when penetrated by NPs.

2.1.4. Enhanced singlet oxygen production by PDT

Since we wanted to have a simple, precise, and reproducible energy source, our approach was to first evaluate different light sources with diverse characteristics in the following order, i.e., broad wavelengths of excitation, unique wavelengths, tailored to requirements of the specific photosensitizer. We wanted to evaluate the robustness of the light sources, so we chose two well-known sensitizers to assess the accuracy and reproducibility of the measurements by calculating the rate of photooxidation and the quantum yield of SO production. Thus, we undertook the task of optimizing the SO production by varying the reaction parameters, such as, concentration of PS, concentration of quencher, solvent, nature and potency of irradiation source, and irradiation time. We used the most commonly quenchers described in the specialized scientific literature: 1,3-diphenylisobenzofuran (DPBF), 2,5-dimethylfuran (DMF), and 2,5-diphenylfuran (DPF) [90, 91]. After optimizing the conditions for PSs to produce SO, we moved to experiments with NPs in order to quantify the production of SO for all the NPs mentioned before, using three methods: spectrophotometry, fluorometry analysis of DPBF oxidation, and analysis of fluorescent probe: singlet oxygen sensor green (SOSG). We choose the standard with the highest production of SO (RB) and a laser on a wavelength of 532 nm because excited nanoparticles and RB are found at this wavelength to trigger photochemical reactions, which produced reactive SO. We measured the intracellular production of SO after the internalization of NPs with and without PDT by a fluorometric analysis of DPBF and analysis of fluorescent probe: singlet oxygen sensor green (SOSG) using a novel method first described by us, which measured the efficiency of the intracellular production of SO by the use of the different NPs with and without PDT. All experiments were made in triplicate.

2.1.5. Apoptosis and cytotoxicity assays of NPs on B-CLL cells

Each of the NPs was tested for apoptotic and cytotoxic effects on B-CLL cells by flow cytometry and propidium iodide/acridine orange vital staining with fluorescent microscopy observation as well as MTT assays, with and without PDT.

2.1.6. Measurement of free ion Zn

Free levels of ion Zn in ultrapure distilled water after incubation with NPs for 24 and 48 h were evaluated by a classical method.

2.1.7. Morphological cell changes after treatment

B-CLL cells and normal lymphocytes were evaluated by light and TEM observation after treatment for cell morphological changes.

3. Results and discussion

3.1. UV-Vis NPs absorption

The optical absorption spectra were recorded in the wavelength region of 200–800 nm. Doping with Mn could increase surface defects of NPs affecting the optical and electronic properties of nanoparticles as well as improving the action of PDT when visible light is used as source. UV-Vis absorption of undoped ZnO and 0.5% Mn-doped ZnO showed a difference in the optical absorption of both the undoped and the Mn-doped ZnO NPs, which could indicate that Mn generates more active sites for reaction at energy level lower than the conduction band of undoped ZnO, and thus absorbs more visible light via these defects sites. Absorption wavelength varies according to the different percentages of doping (Table 1) the optical band gap of undoped and Mn-doped ZnO NPs. Doping ZnO NPs with 0.5% of Mn would contribute with tail states in the vicinity of the valence band owing to the defect sites and reduces its effective band gap.

NPs	Estimated optical band gap (eV)
ZnO	3.5
ZnO:Mn^{+2} 0.5% doping	3.4
ZnO:Mn^{+2} 1.0% doping	3.6
ZnO:Mn^{+2} 1.5% doping	3.54
ZnO:Mn^{+2} 2.0% doping	3.50

Table 1. Optical band gap of undoped ZnO and Mn-doped ZnO NPs at different percentages

http://dx.doi.org/10.5772/61796

3.2. Photoluminescence measurements

The emission spectra of all these NPs had one weak band in the UV region around 397 nm that could be attributed to their band gap as well as another broad one at 542 nm in the visible region, which could be related to oxygen defects. The visible emission is the dominant feature of the luminescence of ZnO and Mn-doped ZnO NPs and results from recombination involving trap states [92]. This increase of fluorescence intensity probably indicates that the incorporation of Mn ions into ZnO NPs may suppress some nonradioactive recombinations of free excitation that is near the band gap emission [92].

3.3. Infrared analysis

An FTIR spectrum of ZnO NPs showed an absorption band centered at 451 cm^{-1} corresponding to the stretching vibration of Zn-O, confirming the formation of a ZnO bound [53, 93], and a vibration band at 1021 corresponding to a C-O bond. The O-H broad stretching band at 3438 cm^{-1} is shown in the spectrum [92, 94]. The intense absorption bands at 1405 cm^{-1} and 1586 cm^{-1} were due to C-C and CH_3COO^- stretching vibrations of carboxylic acid, respectively [95]. The strong presence of those bands at 1405 and 1586 could be attributed to the formation of a zinc acetate solution complex in ethanol, occurring during the synthesis process [96]. The Fourier transform infrared (FTIR) spectrum of the 0.5% Mn-doped ZnO NPs has an intense band at 446 cm^{-1}. This peak confirms substitution of Zn^{+2} ions by Mn^{+2} ions in the crystal structure. The photoluminescence studies illustrated that the doping with Mn modifies the emission properties of ZnO NPs.

3.4. XRD analysis

The average crystalline size of NPs was 7.78 ± 0.9 nm and was determined using the Debye–Scherrer formula [97, 98]. The average crystallite sizes are presented in Table 2. From the results of the XRD analysis of Mn-doped ZnO NPs, we observed that the crystal size increases with doping up to 0.5%, indicating the incorporation of Mn in the ZnO lattice. This phenomenon is shown in Table 4, where the lattice parameters of Mn-doped NPs at different atomic percentages in the 0–2 at.% range were slightly higher than those of undoped ZnO NPs. Any other impurities were detected. In Table 3, the average crystallite sizes of Mn-doped ZnO NPs synthesized at all the different dopant atomic percentages in the 0–2 at.% range are presented.

Percentage of Mn doping of ZnO NPs	Average crystallite size ± standard deviation (nm)
ZnO undoped	7.78 ± 0.9
0.5% Mn^{+2}-doped ZnO NPs	14.41 ± 0.8
1.0% Mn^{+2}-doped ZnO NPs	13.25 ± 0.8
1.5% Mn^{+2}-doped ZnO NPs	11.45 ± 0.7
2.0% Mn^{+2}-doped ZnO NPs	10.95 ± 0.6

Table 2. Average crystallite size of ZnO NPs doped at different Mn atomic percentages in the 0–2 at.% range

Lattice Constants (A°)	ZnO	ZnO:Mn 0.5%	ZnOMn 1.0%	ZnO:Mn 1.5%	Zno:Mn 2.0%
a=b	3.231	3.232	3.245	3.260	3.271
c	5.092	5.174	5.193	5.212	5.236

Table 3. The lattice constants calculated from XRD data of ZnO and different Mn atomic cm^{-1} with percentages in the 0–2 at.% range

3.5. TEM, SEM, and EDS analysis of NPs

By scanning electron microscopy (SEM) and transmission electron microscopy (TEM) after being well deagglomerated using human serum albumin (HSA) and intense sonication [99], most of the nanoparticles had spherical shapes and a well-ordered morphology. Highly monodispersed NPs with an average size of 22.4 ± 1.6 nm were clearly observed (Figures 1 and 2). The resulting ZnO and 0.5% Mn-doped ZnO NP morphology was quite similar when observed by both analysis (TEM and SEM), constituting a homogeneous population of NPs of that mentioned size (Figures 1 and 2). TEM and SEM images showed that the NPs appeared a little larger in size than the same estimated result from Scherrer analysis [100]. In Table 4, the experimental Mn concentration was compared to that obtained by the EDS analysis; being quite similar, this confirms the atomic percentage of Mn present in the ZnO nanoparticles.

% Mn (Theorical)	%Mn (EDS)
0	0
0.5	0.4

Table 4. Theoretical Mn content of 0.5% Mn-doped ZnO NPs and that determined by EDS in the same NPs.

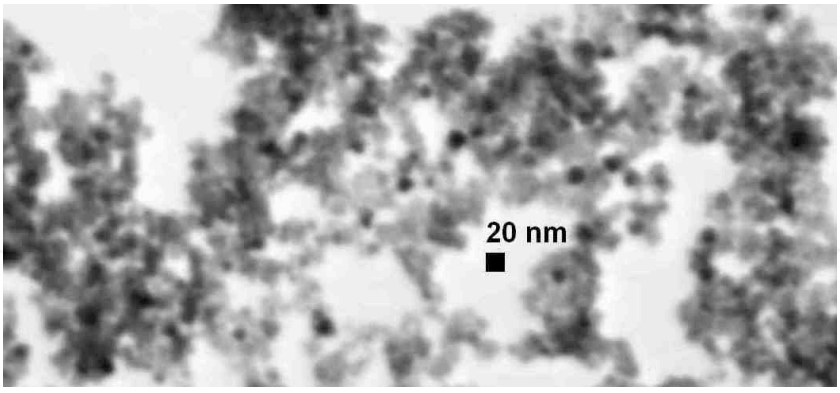

Figure 1. TEM picture of 0.5% Mn-doped ZnO NPs, where they are seen with strong black color, with spherical morphology and uniform size. The gray background is produced by the human albumin used to disperse the particles.

http://dx.doi.org/10.5772/61796

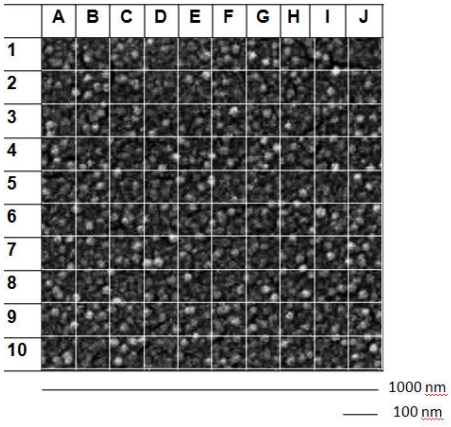

Figure 2. SEM observation of 0.5% Mn-doped ZnO NPs with a counting grid of 1000 × 1000 nm with small square sections of 100 × 100 nm to characterize NPs distribution and size.

3.6. Analytical methods for determination of SO production

Similar results were obtained by the three analytical methods for NPs of 1.0 Mn-doped ZnO. Comparing the spectrophotometric method and fluorometry analysis of DPBF oxidation, similar results were obtained for NPs of 1.0% and 1.5% Mn-doped ZnO and 1.0% Mn-doped ZnS NPs. Core shell ZnO/ZnS did not produce SO at all (Table 5). The measurement of singlet oxygen was similar for ZnO nanoparticles and 1.0% and 2.0% Mn-doped ZnO NPs by both fluorescence methods. Comparing the spectrophotometric method and analysis of fluorescent probe, singlet oxygen sensor green (SOSG), similar results were obtained for NPs of 1.0% Mn-doped ZnO and ZnS.

NPs	Φ_Δ SO by Spectrophotometry analysis	Φ_Δ SO by fluorometry analysis of DPBF oxidation	Φ_Δ SO by analysis of fluorescent probe: SOSG
ZnO	N.R	0.71 $p<0.05$ *	0.66 $p<0.05$ *
ZnO:Mn 0.5% doping	0.60 $p<0.05$ *	0.48	0.74
ZnO:Mn 1.0% doping	0.32	0.28	0.32
ZnO:Mn 1.5% doping	0.17	0.17	0.30
ZnO:Mn 2.0% doping	N.R	0.1	0.17
ZnS	0.36	0.22	0.39
ZnS:Mn 1.0% doping	0.20	0.23	0.52

Table 5. SO quantum yield of NPs by spectrophotometric and fluorometric analysis of DPBF oxidation and by analysis of fluorescent probe: singlet oxygen sensor green (SOSG) in water

We measured the generation of SO in all experiments using NPs and laser irradiation at a wavelength of 532 nm following three different analytical methods: spectrophotometry and fluorometry analysis of DPBF oxidation as well as by the use of a fluorescent probe: singlet oxygen sensor green (SOSG). A standard photosensitizer, RB, of a known SO quantum yield was used to calculate the SO QY of the NPs. Singlet oxygen quantum yield of rose bengal was always significantly higher compared with the QY of any of the NPs used. Anyway, as NPs could have several advantages, that will be explained later on when compared to PSs such as RB. Our results will surely be of great importance for the future clinical application of ZnO NPs. It was clearly demonstrated that the decomposition of DPBF by SO induced by 1.0% Mn-doped ZnO and ZnS NPs at 1.0 mg/mL under laser irradiation conditions was always a time-dependent phenomenon. Comparing both the spectrophotometric method and the fluorometry analysis of DPBF oxidation, similar results were obtained for NPs of 1.0% and 1.5% Mn-doped ZnO and 1.0% Mn-doped ZnS NPs. Our core shell ZnO/ZnS NPs did not produce SO at all. The measurement of SO generation was similar for ZnO nanoparticles and 1.0% and 2.0% Mn-doped ZnO NPs by both fluorescence methods. Comparing the spectrophotometric method and singlet oxygen sensor green (SOSG) routes, similar results were obtained for NPs of 1.0% Mn-doped ZnO and ZnS NPs. In all the other experiments performed in similar conditions, we always found a significant higher generation of SO when 0.5% Mn-doped ZNO NPs were used, and these results seem to indicate that this kind of NP could be the most appropriate to use in living models when SO generation could be needed as a therapeutic strategy. Then the most interesting sample tested in order to use in further experiments with living cells, animal models, or even patients as a potential intracellular SO generator should be 0.5% Mn-doped ZnO NPs, which generated the highest amounts of SO compared to the other Mn-doped samples at 1%, 1.5%, and 2%. These features make 0.5% Mn-doped ZnO nanoparticles potential potent photosensitizers for a combine treatment with PDT. Results for all NPs by the three analytical methods are presented in Table 6. The highest values of SO QY was 0.60 by the spectrophotometric method and 0.74 by SOSG using 0.5% Mn-doped ZnO NPs ($p < 0.05$) and 0.71 by the fluorescence method of DPBF oxidation using ZnO NPs ($p < 0.05$). When a dopant is introduced into a nanoparticle like the ones presented here, a range of percent doping may be most effective in a specific desire clinical action like anticancer selective activity. Additionally, it may be the case that the most effective percent range depends on the nanoparticle composition and the dopant composition. In our case, 0.5% Mn^{+2}-doped NPs had the highest effectiveness in the production of SO. This may be explained in terms of their optical properties with the presence of this doping. Higher fluorescence in the visible region as compared to those Mn^{+2}-doped NPs at 1.0%, 1.5%, and 2.0%. 0.5% Mn^{+2}-doped ZnO NPs generated more SO due of the special transitions in the d orbitals of Mn^{+2}, favoring the photocatalytic processes. At this percentage, the optical and electronic properties of the NPs were favorable for PDT. In this way, there is more energy transfer between the excited NPs with triplet oxygen to produce SO. It is known that these NPs have a good capacity to donor energy and can act as novel PSs in the use of PDT for cancer treatment [28, 50, 101]. The QY of SO by spectrophotometry was 0.60 and 0.48 by fluorometry analysis of DPBF oxidation and 0.74 by analysis of fluorescent probe, respectively. With increasing doping of ZnO NPs from 1.0% to 2.0%, the production of SO decreased in all methods. ZnS NPs without Mn doping

http://dx.doi.org/10.5772/61796

when compared to 1.0% Mn-doped ZnS NPs showed an increased SO production by the spectrophotometric method. The results were similar for ZnS and 1.0% Mn-doped ZnS by the fluorometric method using DPBF oxidation. In the SO detection method using the Sensor Green, Mn-doped ZnS NPs show a considerable increase in the production of singlet oxygen compared to undoped NPs. In general, all NPs have a good production of SO and can be used as efficient PS in PDT except ZnO/ZnS core shell. We made a comparative extensive study with 3 different analytical methods: spectrophotometry, fluorometry analysis of DPBF oxidation, and analysis of fluorescent probe: singlet oxygen sensor green (SOSG), using a novel method first described by us, which measured the efficiency of the intracellular production of SO by the use of the different NPs with and without PDT. There is no current scientific literature of this kind doing comparative studies of the intracellular production of SO, making our group the pioneers worldwide. For the results obtained with our 0.5% Mn-doped ZnO NPs, we certainly believe that this specific doping level generates new unique electrical and luminescence properties in our ZnO NPs for this particular concentration of Mn most probably related to a specialized way of tumor cell death called autophagy, which seems to be the specific result of the intracellular action of metal ZnO NPs at this Mn doping level. The Mn^{+2} dopant atomic percentage of 0.5% for ZnO NPs should be interacting with the molecular and electrical configurations of these Zn NPs in such a way that SO generation is clearly enhanced especially when PDT is used. This could be an interesting and innovative mechanism to be fully discovered and achieved in cancer treatment, especially when low concentrations of Mn doping are used in ZnO NPs associated to PDT [33, 48]. It could be important to look in future studies into the behavior of ZnO NPs when doped with concentrations lower than 0.5% especially at the mitochondrial cell level where many of the respiratory and energy generation processes of the cell are taken place. As shown in our experiments, higher concentrations over 0.5% seem not to improve SO generation or leukemic cell death. In this way, it was thought that these NPs made of Mn-doped ZnO could be used in the treatment of B-CLL and other indolent lymphomas, alone or in combination with PDT. These NPs, when excited by light emission, may generate ROS, especially SO, which could lead to an induced apoptotic process or some other kind of death pathway like autophagy in B-CLL cells, including those with resistant phenotypes to conventional therapies [57]. This strategy could be a very specific one, considering that the oxidative stress found in leukemic cells is supposed to be a lot much higher than that of normal B lymphocytes [102, 103]. Based on a growing body of evidence, ROS production is proposed as a key cytotoxic mechanism mediated by ZnO NPs leading to cell death [104, 105]. The photoactivation of these ZnO NPs was predicted to induce greater levels of ROS, including intracellular SO that we measured by an innovative method developed in this research. This enhanced intracellular generation of SO, if effectively targeted to cancer cells by our Mn-doped ZnO NPs, could produce their selective final destruction [106, 107].

3.7. Intracellular measurement of so production after treatment with NPs with and without PDT

Each of the NPs was tested for apoptotic and cytotoxic effects in B-CLL cells as assayed by flow cytometry and propidium iodide/acridine orange staining as well as MTT assays. It is clear by the results of our experiments that the lowest concentration of Mn doping (0.5%) could

play the most important role in enhancing the cytotoxic effects of our NPs of the present research. These NPs seem to be very selective in their cytotoxic effects toward diseased B-CLL. Our most effective NPs have been synthesized or modified by a method that affects its biological behavior by the addition of a dopant in a concentration that basically could change their redox potential [85, 108]. These parameters could allow for influence same NPs and/or a preferential association of the NPs with a diseased cell. Fluorescence spectra photooxidation of DPBF in the presence of NPs inside B-CLL cells and DPT treatment showed that DPBF reacts with SO, causing a progressive decrease in the intensity of the quencher again. This decomposition of DPBF by SO produced by the use of 1.0% Mn-doped ZnO NPs 3 and ZnS NPs 6 in B-CLL cells was a time-dependent phenomenon (Figures 3 and 4) with an increased production of intracellular SO in B-CLL cells when PDT was delivered. The intracellular singlet oxygen QY of RB was significantly higher compared with QY of NPs (Figures 3 and 4; $p < 0.05$). The quantum yield of SO for B-CLL cells was 0.16 for NPs3 and 0.21 for NPs6 using DPBF as the chemical quencher (Table 6).

SO QY	B-CLL Lymphocytic cells
NP 3	0.16
NP 6	0.21

Table 6. Singlet oxygen (SO) quantum yield (QY) of NPs in B-CLL lymphocytic cells

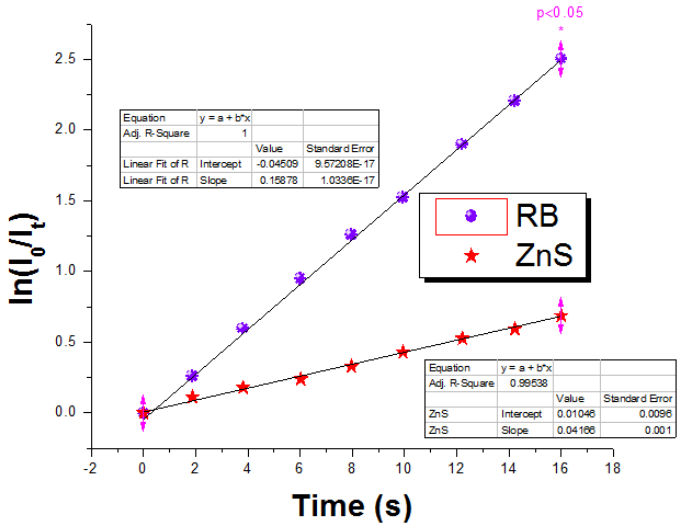

Figure 3. Time-dependent decomposition of DPBF at 6.0×10^{-5} M by SO produced by ZnS NPs at 15 μg/mL and RB at 1.0×10^{-5} M and incubated with B-CLL cells (4 million/2 mL PBS) and irradiated with a green laser 532 nm at a distance of 40 cm up to 16 s every 2 s compared to that produced by RB under same experimental conditions.

http://dx.doi.org/10.5772/61796

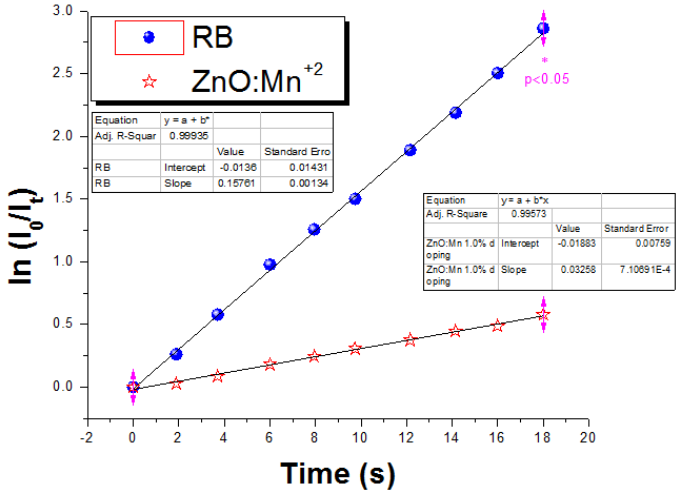

Figure 4. Time-dependent decomposition of DPBF at 6.0×10^{-5} M by SO produced by 1.0% Mn-doped ZnO NPs at 15 μg/mL and RB at 1.0×10^{-5} M and incubated with B-CLL cells (4 million/2 mL PBS) and irradiated with a green laser 532 nm at a distance of 40 cm up to 18 s every 2 s compared to that produced by RB under same experimental conditions.

3.8. Penetration of cells by NPs

We first evaluated the effect of three different doses (0.1, 0.2, and 0.3 mg/mL) of each of the 8 NPs produced by testing them in their penetration capacity into B-CLL cells as well as into normal B lymphocytes during a total culture period of 3 h (Fig 5). The results of these experiments indicated that 0.2 mg/mL of each of the analyzed NPs resulted in an intense cell penetration activity that was not further increased by its rising to a higher concentration of 0.3 mg/mL. Because of this, the concentration of 0.2 mg/mL of NPs was used in all further experiments. At zero time, no particles were seen inside any of the cells (Fig 6a), but at 2 h time point, all observers agreed that there was a maximum "intense" similar penetration of all NPs in both types of cells (Figure 6b). Normal lymphocytes as well as B-CLL cells were well and maximally penetrated by NPs at 0.2 mg/mL concentration when cultured at 37°C during 2 h and observed under TEM (Figure 6b). At 3 h culture time, no further significant increase in the amount of total NP penetration into cells was observed in either leukemic or normal ones. B-CLL cells as well as normal B lymphocytes when incubated during this time period with 0.2 mg/mL of each of the NPs and observed under TEM and fluorescent microscopy were clearly and intensively penetrated by all of these NPs tested as described by the 3 observers, and no increment of NP penetration in cells was found after this time point as it was said. In this way, an incubation period of 120 min with 0.2 mg/mL of NPs was selected as the best conditions for NP penetration into cells.

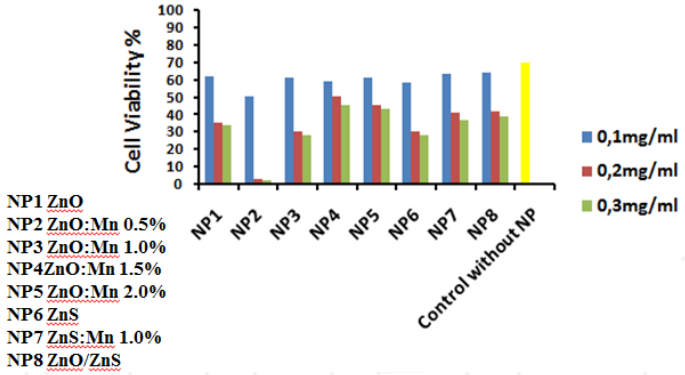

Figure 5. Effect of three different doses of each of the 8 NPs tested on the viability of B-CLL cells at 48 h of incubation after PDT. The dose 0.2 mg/mL produced the most intense killing activity. Increasing this dose up to 0.3 mg/mL did not produce further significant increase in cell mortality as seen with 0.2 mg/mL.

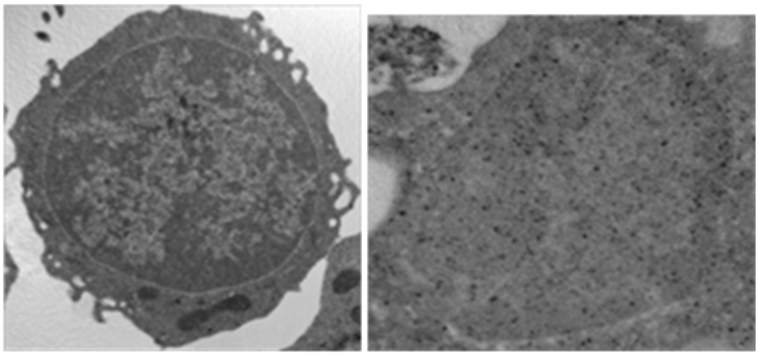

(a) (b)

Figure 6. (a) B-CLL cell in culture with no NPs observed with TEM at time 0. Penetration degree: none. (b) B-CLL cell penetration by 0.5% Mn-doped ZnO NPs observed at 2 h by TEM. Penetration degree: intense. As panel b suggests, the NPs also penetrated the cell nucleus.

3.9. Cell viability and mortality testing

Then we evaluated the effect of those same three different doses (0.1, 0.2, and 0.3 mg/mL) of each of the 8 NPs produced on the viability of B-CLL cells at 24 and 48 h of incubation after PDT (Fig 5). In these probes, 0.2 mg/mL of each of the NPs tested again resulted in the best B-CLL cell killing activity. Normal lymphocytes also had the greatest mortality rates at this NPs concentration but were always significantly lower and mostly insignificant in relation to that observed for B-CLL cells. It was also seen that 0.1 mg/mL of each NP had almost no significant difference in the viability of B-CLL cells in relation with that of the control samples without NPs. In this way, this concentration did not seem to be the best one to be tried in further

experiments. Scaling up the NPs concentration to 0.3 mg/mL did not either significantly improved the cell killing activity of those same NPs in relation to that concentration of 0.2 mg/mL. Then this concentration of 0.2 mg/mL was selected and used for all other experiments. From the 8 NPs especially designed and produced for this study, 0.5% Mn-doped ZnO NPs were chosen as the most powerful killing NPs against B-CLL cells when associated with PDT but with minimum impact on normal lymphocytes. At the mentioned concentration of 0.2 mg/mL, NPs2 (0.5% Mn-doped ZnO NPs) were the most effective NPs in relation to its killing activity of B-CLL cells (Fig 7). In this way, NP2 was selected for the performance and cytotoxicity procedures.

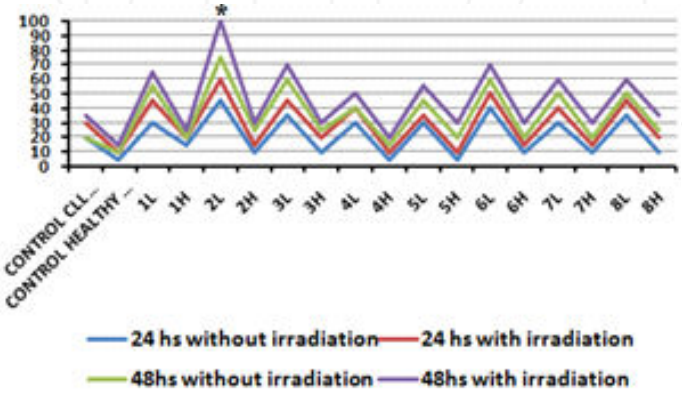

Figure 7. Cytotoxicity levels of B-CLL cells (L) from 5 patients and normal B lymphocytes (H) from 5 healthy donors for each NP at 24 and 48 h with and without laser irradiation. Clearly, the most intense mortality is observed in B-CLL cells exposed to NPs2 at 48 h and laser irradiated.

3.10. Intracellular so production determinations

Changes in the production of intracellular SO were determined in both normal and B-CLL cells after being penetrated by NPs and laser irradiated. The increase of intracellular SO was significantly higher in B-CLL cells than in normal B lymphocytes. Measurements of the intracellular SO generation quantum yield after PDT was done by fluorometry quantitative analysis of photooxidation reactions using either DPBF as the quencher or SOSG as a fluorescent probe for singlet oxygen, as previously described. B-CLL cells as well as normal B lymphocytes when incubated during 2 h with SOSG and observed under fluorescent microscopy were clearly penetrated by this fluorescent probe. The measurement of the intracellular fluorescence spectra of SOSG in the presence of 0.5% Mn-doped ZnO NPs inside B-CLL cells and normal B lymphocytes was possible by using our described method and by recording its changes every minute up to 7 min upon irradiation (Figure 8). A selective increase in the intensity of the fluorescence of SOSG especially in B-CLL cells as a result of the larger production of intracellular SO induced by the action of light when these 0.5% Mn-doped ZnO NPs have already penetrated these cells was recorded. SO quantum yields were determined with

the graph of time dependent of SOSG in the presence of NPs inside cells after PDT (Figure 9). A quantitative comparison of the intracellular SO generation between normal lymphocytes and B-CLL cells, both treated with Mn 0.5%-doped ZnO NPs and PDT, using this SOSG fluorescent probe, showed a significant increase in SO generation in malignant leukemic cells rather than in normal ones (Figure 10a and b). The quantum yield was calculated using Equation (1) [91], and the values were 0.88 in B-CLL cells and 0.49 in normal lymphocytes using SOSG as a fluorescent probe for singlet oxygen, as previously described.

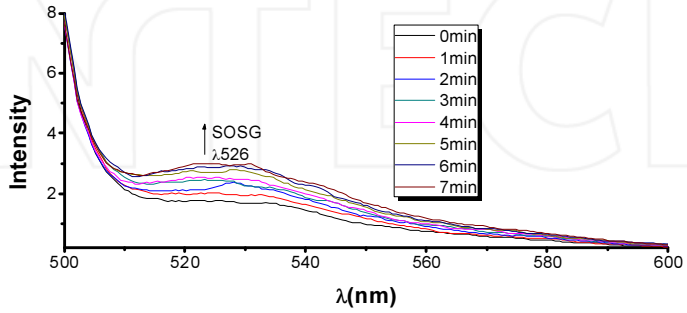

Figure 8. Intracellular PL spectra of SOSG at 5 μL/mL from B-CLL cells (4 million/2 mL PBS) penetrated by of 0.5% Mn-doped ZnO NPs at 0.2 mg/mL, while the cellular suspension was irradiated with a green laser 532 nm at a distance of 40 cm every minute up to 7 min. The excitation wavelength was 488 nm. The increase in the fluorescence intensity of SOSG as a function of time irradiation is clearly observed. There was no interference in the measurements produced by the cells.

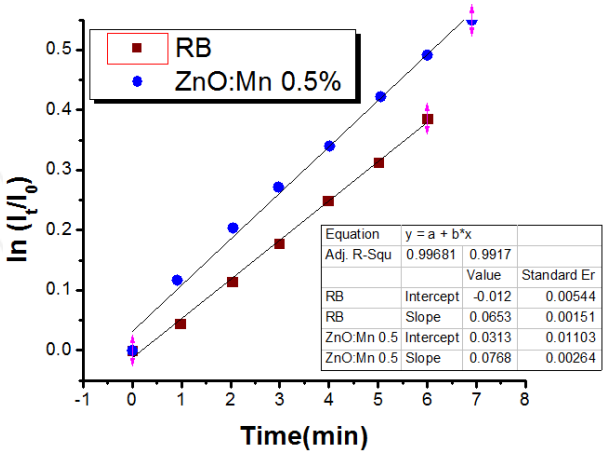

Figure 9. Time dependent of SOSG at 5 μL/mL by SO produced by 0.5% Mn-doped ZnO NPs at 0.2 mg/mL and RB at 1.0×10^{-5} M and incubated with B-CLL lymphocytic cells (4 million/2 mL PBS) while irradiating with a green laser 532 nm at a distance of 40 cm up to 7 min every 1 min.

http://dx.doi.org/10.5772/61796

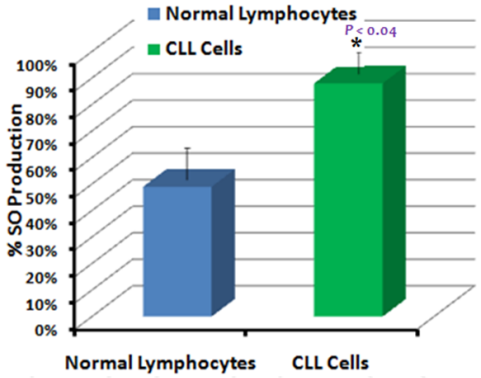

(a)

SOSG QY	Lymphocytes	B-CLL Lymphocytic cells
ZnO:Mn $^{+2}$ 0.5% doping with HSA	0.49	0.88

(b)

Figure 10. (a) Quantitative comparison of the intracellular SO generation after PDT by a fluorescent probe SOSG between normal lymphocytes and B-CLL cells from 5 healthy donors and 5 CLL patients treated with 0.5% Mn-doped ZnO NPs. (b) Singlet oxygen sensor green (SOSG) quantum yield (QY) of Mn 0.5%-doped ZnO NPs inside normal lymphocytes and B-CLL cells.

B-CLL cells as well as normal B lymphocytes when incubated during 2 h with SOSG and observed under fluorescent microscopy were clearly penetrated by this fluorescent probe. The measurement of the intracellular fluorescence spectra of SOSG in the presence of 0.5% Mn-doped ZnO NPs inside B-CLL cells and normal B lymphocytes was possible using our described method and recording its changes every minute up to 7 min upon irradiation (Figure 8). A selective increase in the intensity of fluorescence of SOSG especially in B-CLL cells as a result of the larger production of intracellular SO induced by the action of light when these 0.5% Mn-doped ZnO NPs have already penetrated these cells was recorded. SO quantum yields were determined with the graph of time dependent of SOSG in the presence of NPs inside cells after PDT (Figure 9). A quantitative comparison of the intracellular SO generation between normal lymphocytes and B-CLL cells, both treated with 0.5% Mn-doped ZnO NPs and PDT, using this SOSG fluorescent probe, showed a significant increase in SO generation in malignant leukemic cells rather than in normal ones (Figure 10a and b). The quantum yield was calculated using Equation (1) [91], and the values were 0.88 in B-CLL cells and 0.49 in normal lymphocytes using SOSG as a fluorescent probe for SO, making this difference significant ($p < 0.04$) (Figure 10a). In Equation (1), $\Phi\Delta_{sample} = \Phi\Delta_{ref} K_{sample} / K_{ref}$, where $\Phi\Delta_{ref}$ is the SO quantum yield of rose bengal (RB) and K_{sample} and K_{ref} are the slopes of the plot of the time-dependent increase of SOSG, expressed as the increase of fluorescence at 526 nm of the measured 0.5% Mn-doped ZnO NPs and the RB, respectively (Figure 9). The other method

used to calculate the production of intracellular SO was that in which DPBF performed as the chemical quencher in a decomposition reaction. In the analysis of DPBF oxidation by SO, K_{sample} and K_{ref} are the slopes of the plot of the time-dependent decomposition of DPBF, expressed as the decrease of fluorescence at 453 nm of the measured 0.5% Mn-doped ZnO NPs and the RB, respectively (Figure 11). In this way, SO production was significantly higher in B-CLL cells compared to normal lymphocytes when both types of cells were treated with NPs and PDT [6, 18, 51] (Figure 12a and b). Fluorescence spectra photooxidation of DPBF in the presence of 0.5% Mn-doped ZnO NPs inside B-CLL cells showed that DPBF reacts with SO, causing a progressive decrease in the intensity of the quencher (Fig 13). This decomposition of DPBF by SO produced by the use of RB and 0.5% Mn-doped ZnO NPs in B-CLL cells was a time-dependent phenomenon, and again there was an increased production of intracellular SO much higher in B-CLL cells than in normal lymphocytes when PDT was delivered (Figure 12a and b). The quantum yield of SO for B-CLL cells was 0.21 and 0.10 for normal lymphocytes using DPBF as the chemical quencher. Then it is clear that a similar phenomenon was observed in both cases when SOSG or DPBF were used.

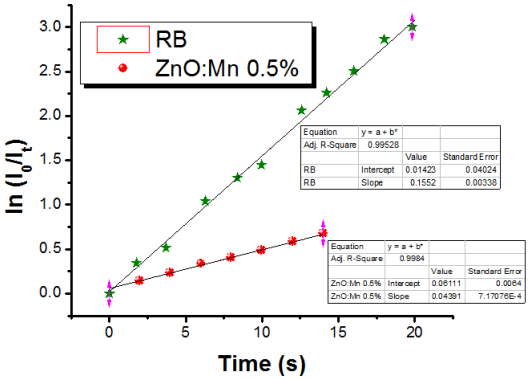

Figure 11. Time-dependent decomposition of DPBF at 6.0×10^{-5} M by SO produced by 0.5% Mn-doped ZnO NPs at 0.2 mg/mL and RB at 1.0×10^{-5} M and incubated with B-CLL cells (4 million/2 mL PBS) and irradiated with a green laser 532 nm at a distance of 40 cm up to 14 s every 2 s.

SO production was found to be increased in both normal and B-CLL cells when cultured with 0.5% Mn-doped ZnO NPs and laser irradiated, but this increase in SO production was always significantly higher in B-CLL cells compared to normal lymphocytes.

3.11. Cytotoxicity levels produced by NP treatment with and without PDT

Cytotoxicity levels produced by each of the NPs described before on B-CLL cells compared to that on normal B lymphocytes at 24 and 48 h with and without laser irradiation was in all cases significantly higher (Figure 14). At the 0.2 mg/mL concentration, NP2 (0.5% Mn-doped ZnO NPs) was the most effective NP in relation to killing activity of B-CLL cells while having a minimum effect on normal B lymphocytes. The 0.5% Mn-doped ZnO NPs effectively elimi-

http://dx.doi.org/10.5772/61796

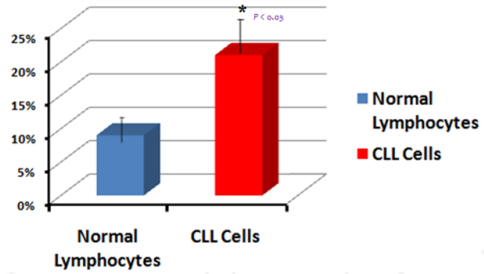

(a)

SO QY	Lymphocytes	B-CLL Lymphocytic cells
ZnO:Mn $^{+2}$ 0.5% doping with HSA (0.2mg/mL)	0.10	0.21

(b)

Figure 12. (a) Quantitative comparison of the intracellular SO generated after PDT by fluorometry quantitative analysis of photooxidation reactions using DPBF as quencher between normal lymphocytes and B-CLL cells penetrated by 0.5% Mn-doped ZnO. (b) Singlet oxygen (SO) quantum yield (QY) generated in normal lymphocytes and B-CLL cells penetrated by 0.5% Mn-doped ZnO after PDT.

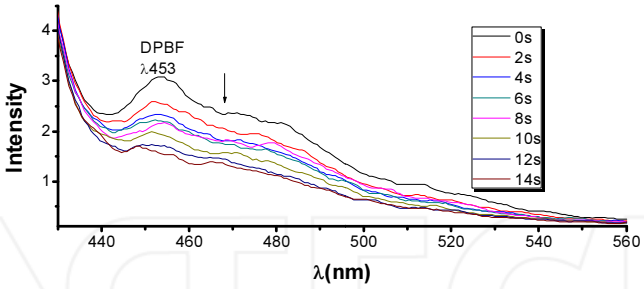

Figure 13. Intracellular PL spectra photooxidation of DPBF at 6.0×10^{-5} M from B-CLL (4 million/2 mL PBS) cells penetrated by 0.5% Mn-doped ZnO NPs at 0.2 mg/mL. The suspension was irradiated with a green laser 532 nm at a distance of 40 cm every 2 and up to 14 s. The excitation wavelength was 410 nm. DPBF reacts with SO, which causes a decrease in the intensity of the quencher. There was no interference in the measurements by the cells.

nated the largest amount of fludarabine-resistant B-CLL cells with almost no lost produced in the viability of normal healthy lymphocytes. The intracellular increase of SO production correlated well with cell mortality, as will be described later. After 24 h in culture, both healthy (H) and leukemia (L) cells without NPs had a spontaneous cell death of 5% and 20%, respectively (Figure 14). Cell irradiation with lasers showed no statistical difference in terms of apoptosis or mortality in both cell populations at this time, when no NPs were used. However,

when cultured during the same period of time, but exposed to Zn NPs, B-CLL cells without irradiation showed an important loss of viability, especially if culturing time is prolonged to 48 h. Percentages of cytotoxicity increased significantly with PDT at 24 and 48 h in B-CLL cells cultured with NPs. The maximum increase in mortality of B-CLL cells was achieved with NPs2 at 48 h when PDT was applied. Our NPs have distinct effects on cell viability by killing B-CLL cells, but it had very few effects on normal lymphocytes. The marked differences observed in cytotoxicity between B-CLL cells and normal lymphocytes especially using the 0.5% Mn-doped NPs suggest a very exciting potential for these NPs as a novel alternative for leukemia treatment, especially when PDT was applied simultaneously. These NPs induce autophagy in B-CLL cells, which is mediated by SO. B-CLL cells are known to have elevated levels of ROS [1, 6, 56]. We aimed to test a novel ROS-mediated strategy to eliminate fludarabine-resistant B-CLL based on this redox alteration. Our study demonstrated that the Mn-doped ZnO NPs with PDT are effective in eliminating fludarabine-resistant B-CLL cells through SO mechanism with low toxicity to normal lymphocytes. Apoptosis levels for irradiated and nonirradiated cells cultured with NPs2 at 24 and 48 h detected by flow cytometric analysis (annexin V/PI double staining) were always significantly higher in B-CLL cells compared to normal lymphocytes (Figure 14). Apoptotic normal B lymphocytes and B-CLL cells at 24 h cultured with NPs2 were 14% and 49%, while these percentages moved up after laser irradiation (PDT) to 28% and 90% ($p < 0.001$), respectively (Figure 14). Comparison of the mean IC50 of 0.5% Mn-doped ZnO on B-CLL cells ($n = 5$) and normal lymphocytes ($n = 5$) clearly showed a significant difference when NPs2 were used to treat B-CLL cells. Fludarabine-resistant B-CLL cells were clearly much more sensitive to NPs2, with an IC50 value of 0.1 mg/mL, while normal lymphocytes had an IC50 value a lot above and significantly higher for that same NP2 of (Figure 15). MTT assays comparing primary B-CLL cells isolated from the blood samples of the 5 CLL patients (L), which were considered clinically fludarabine resistant with unmutated Ig VH and that of normal B lymphocytes from healthy subjects (H) sensitivity to the action of NPs, clearly showed that the dose response to NPs2 in the fludarabine-resistant B-CLL cells was significantly greater than that observed in normal lymphocytes (Figure 14). SO production was found to increase in both normal and B-CLL cells when cultured with NPs2. This increase in SO production was significantly higher in B-CLL cells compared to normal lymphocytes. This increased intracellular SO production correlated well with cell mortality (Figure 16).

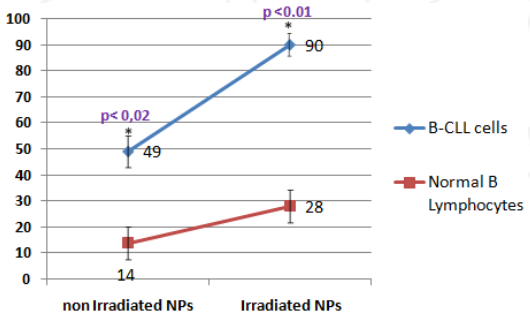

Figure 14. Apoptosis levels for irradiated and nonirradiated B-CLL cells and normal B lymphocytes cultured with 0.5% Mn-doped ZnO NPs (NPs2) at 24 h detected by flow cytometric analysis (annexin V/PI double staining)

http://dx.doi.org/10.5772/61796

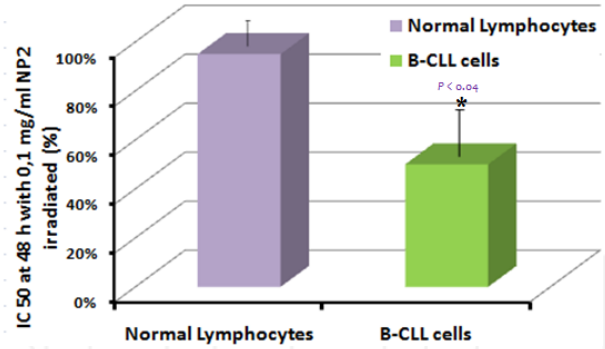

Figure 15. Comparison of the mean IC50 of 0.5% Mn-doped ZnO NPs on B-CLL cells ($n = 5$) and normal B lymphocytes ($n = 5$).

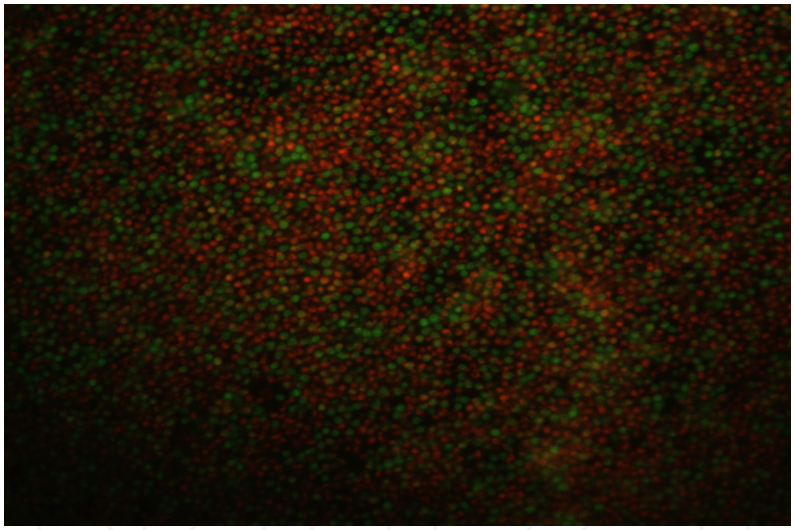

Figure 16. Mortality/viability levels of B-CLL cells incubated with 0.2 mg/mL of 0.5% Mn-doped ZnO NPs for 48 h and PDT. Observed under fluorescence microscopy with FluoroQuench (acridine orange/propidium iodine: 95% mortality).

Mortality/viability levels of B-CLL cells incubated with different NPs were tested using our FluoroQuench method as well with MTT and flow cytometry techniques, as explained before. The results were similar no matter the technique used; the incubation of B-CLL cells with 0.2 mg/mL of 0.5% Mn-doped ZnO NPs for 48 h and PDT produced the highest level of cell mortality (Figure 16). Also, as it has been described in Chapter 4.1.10, in every case, cells were used for cell viability testing normal and B-CLL cells without NPs were always used as blanks or controls samples.

3.12. Measurement of free ion Zn after incubation of cells with NPs

No dosable free ion Zn was measured in the ultrapure water with NPs2 after 72 h of incubation. Tests of cytotoxicity with the possible amount of free ion Zn that could have been determined in these measurements were not further necessary as no free Zn was detected at all in the analyzed ultrapure water.

3.13. Morphological cell changes after treatment with NPs with or without PDT

As observed by optical and fluorescent microscopy, but especially by TEM, and photographed (Figure 17), both types of cells could undergo a process of cell death after 0.5% Mn-doped ZnO NP treatment with or without PDT, corresponding to features of autophagy, but this phenomenon was always stronger when PDT was applied. This autophagic cell death was especially pronounced, much more advanced, massive, and faster on B-CLL cells, affecting almost all of them treated in this way (Fig 17). In the other hand, normal B lymphocytes only suffered autophagic changes in a very lesser degree and basically in the form of an isolated pattern in which only few cells went through this dying pathway besides being treated in the same way and during the same period of time. In this scenario of autophagy, the formation of double membrane-bound organelles predominated in B-CLL cells when treated with 0.5% Mn-doped ZnO NPs alone but predominantly when PDT was simultaneously applied. These organelles were clearly autophagosomes, and by this specific detail, the observed dying process can undoubtedly be considered as autophagy (Figure 17), which denotes any cellular pathway involving the delivery of cytoplasmic material to the lysosome for degradation [109, 110, 111].

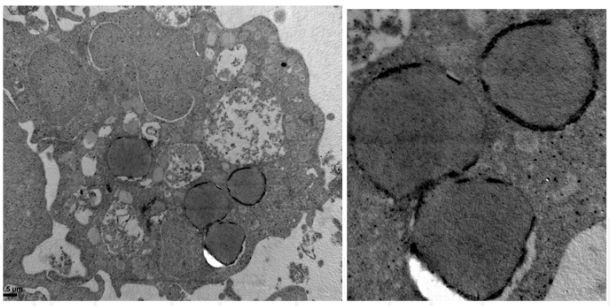

Figure 17. Thin-section TEM images of formation of double membrane-bound organelles in a B-CLL cells when treated with 0.5% manganese-doped ZnO NPs and PDT. These organelles are autophagosomes, and the cell dying process is undoubtedly autophagy

4. General conclusions

In this study, light parameters were primarily evaluated (e.g., intensity of light, broad vs. specific wavelength, and coherent vs. noncoherent nature of light source) for the PSs and

http://dx.doi.org/10.5772/61796

quenchers selected to enhance their effect on SO production. The indirect method using DPBF and DPF as quenchers of SO was tested with different light sources incorporating variations in their intensity. Different coherent and noncoherent light emissions with broad and specific wavelength characteristics were used, finding useful and reliable correlations with enhanced generation of SO species in methanol and water. All this information was of great importance for the in vitro studies later on performed as the corresponding SO quantum yields in each case were elucidated and confirmed. Our results clearly suggest the strong influence of the LED lasers and light power intensities on the quantum yield of SO in the presence of different PS–quencher photooxidation pairs under simultaneous aeration in methanol and water. The best results in these circumstances were obtained with specific wavelength LED lasers, which allowed the exact selection of wavelengths and the precise application of light in contrast to lamps, LED flashlight, and fluorescent light bulbs. Considering that PDT depends largely on the light source, the choice of the emission wavelength could usually range from 350 to 1100 nm, depending on the area of the tumor to be treated. In our case, after performing many systematic experiments on the effects of LED lasers of different intensities as excitation sources on SO quantum yields, we choose a laser on a wavelength of 532 nm because at this wavelength are excited nanoparticles to trigger photochemical reactions, which produced reactive SO that killed BCLL by autophagy. Important data between fundamental physical properties of light sources and enhanced SO production using standard sensitizers and inorganic NPs have also been found and analyzed in order to characterize for the reliable, precise, and reproducible measurement and employment of SO in cancer treatment, especially B-CLL. The quantum yield of SO production via sensitization may be given by the sum of contributions due to O_2 quenching of S1 and T1, the lowest excited singlet and triplet states of the PS. Values of $\phi\Delta$ depend on solvent, reaction conditions, light source, measurement technique, and concentration of O_2. Values obtained here are very consistent with the literature for RB and MB using different quenchers or scavengers. We obtained very good results in agreement with the literature, where the QYs of SO were 0.75 for RB and 0.5 for MB using RNO with L-histidine or imidazole as chemical scavengers in both cases. SO reacts with L-histidine or imidazole via a Type II mechanism, in which SO is generated via an energy transfer process. As a very interesting and novel contribution, NPs were found to be able to participate in the actual mechanisms of PDT, mainly by acting as photosensitizers themselves and clearly enhancing SO generation extra- and intracellularly. We produced and tested a variety of metal Zn NPs with good properties for SO generation, of which one made of 0.5% Mn-doped ZnO (0.5% Mn-doped ZnO) had the best killing activity in fludarabine-resistant and unmutated Ig VH B-CLL cells, especially when combined with PDT. Some nanomaterials like this last one can generate and enhance SO inside and outside the cells, with and without PDT, but especially if it is used. Although this area has not received as much attention as the application of nanomaterials to electronics or catalysis, it represents a promising route to overcoming many of the difficulties associated with traditional PDT. Quantum dots meet the first five criteria for good PSs: they are compounds with constant composition, are not cytotoxic in the absence of light, but have a potential to induce cytotoxicity with and even without UV irradiation. The intracellular delivery of QDs can be facilitated by surface coatings, and they can be functionalized to be both water soluble and biocompatible. The synthesis of different immunocompatible QD

bioconjugates (e.g., QD-cluster-of-differentiation (CD) antibodies) can guarantee their specific localization into target tissues. One benefit of their unique optical properties is that they can be precisely tuned from the UV to the infrared (IR) region of the spectrum by changing their size and composition. Their emission properties result from quantum-confinement effects and can be tuned to emit into the near-IR region in contrast to the visible emission of the most conventional PSs. Furthermore, because of their large transition dipole moment, QDs are strong absorbers, making them potential candidates for application in photodynamic processes, which has been clearly demonstrated in our B-CLL cell tests, also specifically inducing the autophagic cell death of these malignant cells especially when PDT is delivered simultaneously. NPs seem to offer the best hope for extending the reach of this promising therapy to regions deep in the body or even the blood in patients with B-CLL. It is clear now that NPs could provide many advantages over those of traditional PS such as RB. These PS have limits, especially in their clinical applications, derived from a very low lipid solubility as well as by their possible intrinsic toxicity due to a high polarity. Then metal NPs, like the ones described here, could be an optional effective treatment for drug-resistant forms of B-CLL and may also be for many other types of malignant tumors like lymphomas. As shown in our results, we measured the generation of SO in all our cell experiments using NPs with and without laser irradiation at a wavelength of 532 nm by three different analytical methods: spectrophotometry and fluorometry analysis of DPBF oxidation as well as by the use of a fluorescent probe: singlet oxygen sensor green (SOSG). A standard photosensitizer, RB, of a known SO quantum yield was used to calculate de SO QY of the NPs. The singlet oxygen quantum yield of rose bengal was always significantly higher compared with the QY of any of the NPs. Anyway, as NPs could have several advantages, compared to PSs such as RB, our results are surely of great importance especially in the translational use of these new technologies. It was clearly demonstrated that there was a significant higher generation of SO when 0.5% Mn-doped ZNO NPs were used, and these results seem to indicate that this kind of NP could be the most appropriate to use in living models when SO generation could be needed as a therapeutic strategy. Then the most interesting sample tested in order to use in further experiments with living cells, animal models, or even patients as a potential intracellular SO generator should be 0.5% Mn-doped ZnO NPs, which generated the highest amounts of SO compared to the other Mn-doped samples at 1%, 1.5%, and 2%. These features make 0.5% Mn-doped ZnO nanoparticles potential potent photosensitizers for a combine treatment with PDT (photodynamic therapy). One important aspect that we consider fundamental at the moment of characterization and in vitro cell testing of NPs of these kinds is its degree of sample agglomeration. For investigations of the in vivo effects of ZnO NPs in the circulation as well as for measuring their effects in vitro, on different cell types, NPs have to be dispersed and deagglomerated well in physiological solutions. However, particles in solutions with physiological salt concentrations and pH values usually form greater-sized coarse agglomerates. Coarse agglomerates of NPs have been shown to exert different biological effects as compared to well-dispersed NPs and could change some of the characterization parameters. Therefore, investigating the biological effects of nanoscaled particles with dispersions containing coarse agglomerates is not appropriate. Previously, different methods have been published on ways to avoid the formation of these coarse agglomerates of NPs dispersed in physiological

http://dx.doi.org/10.5772/61796

solutions. The importance of the correct ultrasound energy as well as the use of dispersion stabilizers should always be emphasized for the optimal deagglomeration of NPs. We tried several procedures described previously in the literature, making human albumin with strong sonication as the most effective for this purpose. As agglomeration could be a crucial point at the moment to perform NPs characterization as well as in vivo cellular probes and its clinical introduction in living organisms, we suggest to take this point in account very seriously in order to not interfere with the results. When NPs are delivered into the circulation of living organisms, they first get in contact with albumin and other serum proteins. These proteins cover the nanoparticles. Our procedure of deagglomeration uses also albumin; thus, NPs dispersed with this method are covered with the same proteins NPs encounter in the circulation. TEM and SEM confirmed our findings as preparation with this optimized method resulted in an improved dispersion and deagglomeration with any of the NPs studied. Doping at 0.5% with Mn^{+2} increases the production of SO, which was attributed to the optical properties of NPs that were changed, and this fact was closely related to the actions of Mn within the doped NPs. The surface traps of these NPs were eventually quenched by the incorporation of Mn and was confirmed by PL emission, a phenomenon that correlated well with the reduction in the surface traps. At higher concentrations of Mn^{+2} than 0.5%, the generation of SO was lower due the greatest loss of fluorescence of the NPs, inducing higher density of defects not favoring energy transfer processes that enter the NPs and oxygen needed in the SO production. When a dopant is introduced into a nanoparticle like the ones presented here, a range of percent doping may be most effective in a specific desire clinical action like anticancer selective activity. Additionally, it may be the case that the most effective percent range depends on the nanoparticle composition and the dopant composition. In our case, 0.5% Mn^{+2}-doped NPs had the highest effectiveness in the production of SO. This may be explained in terms of their optical properties with the presence of this doping, higher fluorescence in the visible region as compared to those Mn^{+2}-doped NPs at 1.0%, 1.5%, and 2.0%. At this percentage, the optical and electronic properties of the NPs were favorable for PDT. Mn-doped ZnO NPs have distinct effects on cell viability by killing B-CLL cells with low toxicity to normal lymphocytes. These NPs induced a predominant process of autophagy, leading to the massive death of B-CLL cells related to a higher production of SO. This type of NPs could selectively and rapidly increase, just by themselves, the intracellular levels of SO in B-CLL cells conducting them to an autophagic death program that could irreversibly kill them easily but very strongly when delivered with PDT. Using this kind of treatment, B lymphocytes persist mostly alive and not harmed at all by these NPs, PDT, or its combination, as it has been proven here. We have seen that very small variations of intracellular SO concentrations in therapy-resistant leukemic cells could execute and accelerate these deadly pathways, being these mechanisms potentiated and increased by the concomitant delivery of PDT, rendering normal cells almost untouched. An interesting and rapid dying process of the B-CLL cells when incubated with these 0.5% Mn^{+2}-doped ZnO NPs clearly corresponding to autophagy always occurred. There was double membrane-bound organelles cell formation known as autophagosomes, seen under transmission electronic microscopy (TEM) and correlating well with those intracellular increases of SO, that we have measured by a novel method first described by us, which was again more intense when PDT was applied. SO is believed to be the major cytotoxic agent involved in PDT. B-CLL

cells are known to have elevated levels of ROS. We aimed to test a novel ROS-mediated strategy to eliminate fludarabine-resistant B-CLL based on this redox alteration. The measurement of SO in biological environments has been a major task, especially when intracellular values, without interferences from the external medium, are required. Near-infrared (NIR) luminescence at 1270 nm in cell environments is confounded by the strongly reduced SO lifetime and probably had never been achieved until a research group developed an NIR-sensitive photomultiplier tube probe that allowed to clearly identify and measure a true intracellular component of SO signal. However, these few described methods are expensive and required of a complex technology to be performed. We developed a comparative extensive study with 3 different analytical methods: spectrophotometry, fluorometry analysis of DPBF oxidation, and analysis of fluorescent probe: singlet oxygen sensor green (SOSG), using a novel method first described by us, which measured the efficiency of the intracellular production of SO by the use of the different NPs with and without PDT. There is no current scientific literature of this kind doing comparative studies of the intracellular production of SO, making our group the pioneers worldwide. We synthesized a series of ZnO nanoparticles with varying concentrations of Mn dopant. Each of the nanoparticles were tested for cytotoxic effects in B-CLL cells as assayed by flow cytometry and propidium iodide/acridine orange staining as well as MTT assays. It is clear by the results of our experiments that the lowest concentration of Mn doping (0.5%) could play the most important role in enhancing the cytotoxic effects of our nanoparticles of the present research. Our intracellular SO measurement method proved to be good enough, inexpensive, and quite simple that it could easily soon be introduced as a routine but very important diagnostic tool. PDT is a clinically tested promising technique to treat cancer and can be associated therapeutically with NPs. Visible emission processes should involve transitions in which the photogenerated holes at the surface of NPs could be trapped by O_2 ions as they are responsible of this phenomenon. Doping with Mn could increase these surface defects of NPs and improve the processes of PDT. The 0.5% Mn^{+2}-doped ZnO NPs2 were able to produce the highest level of cytotoxicity and apoptosis in unmutated B-CLL cells as compared to normal lymphocytes that were quite resistant to this type of therapy, especially after being irradiated with a green laser ($p < 0.01$). This differential effect could be due to changes observed by several authors in the redox state of leukemic and other neoplastic cells respect to normal ones. The fact that unmutated B-CLL cells responded strongly to the cytotoxic effect of these 0.5% Mn-doped ZnO NPs after PDT is also very important, suggesting that this novel therapy with modifications could be used may be soon, as an alternative effective treatment especially under the occurrence of B-CLL-resistant phenotypes. The 0.5% Mn-doped ZnO NPs combined with PDT show much promise as a new anticancer therapy, given the specific autophagic responses triggered in these leukemia cells. It is also interesting to mention the fact that the best killing results were obtained with the lowest Mn doping concentrations. This fact could open the door to future studies with even lowest amounts of this doping agent in the search of the best NP design. NPDT uses light to activate light-sensitive drugs (photosensitizers) to produce short-lived cytotoxic species such as SO to destroy malignant cells. We investigated the mechanisms of cell death during PDT using fluorescence microscopy and imaging and performing fluorometric measurements to help design the better treatments for resistant forms of B-CLL. We can envision external devices for blood irradiation

http://dx.doi.org/10.5772/61796

by PDT after NP treatments, although "intelligent" ZnO NPs with self-assemblies for energy discharge and light emission from their same structure or "hybrids" of biodegradable shell nanoparticles coated with specific monoclonal antibodies are being loaded in their core with Zn nanoparticles. As this therapy seems to be very specific to fludarabine-resistant B-CLL cells, without much or any damage made at all to normal lymphocytes, it could contribute as a new innovative targeted strategy in the near future to be delivered in the clinical setting for the definitive benefit of these bad prognostic patients. As normal B lymphocytes are much more resistant than B-CLL cells to the cytotoxic effect of NPs with PDT, we could call this new therapeutic approach as a very specific one with very low toxicity for nonleukemic cells and probably very useful not only for B-CLL but also for all the other indolent lymphomas as well as for all types of cancer.

Author details

Sandra Loydover Peña Luengas[1*], Gustavo H. Marin[2], Luis Rivera[1], Adrian Tarditti[2], Gustavo Roque[2] and Eduardo Mansilla[2]

*Address all correspondence to: sandraluengas@yahoo.es

1 Chemistry Department, University of Puerto Rico at Mayaguez Campus, Puerto Rico, USA

2 Tissue Engineering, Regenerative Medicine and Cell Therapies Laboratory, CUCAIBA, Ministry of Health, Province of Buenos Aires, Argentina

References

[1] M. Palma, P. Kokhaei, J. Lundin, a Choudhury, H. Mellstedt, and a Osterborg, "The biology and treatment of chronic lymphocytic leukemia," *Ann. Oncol.*, vol. 17 Suppl 1, pp. x144–54, Sep. 2006.

[2] C. SHERR, "Principles of tumor suppression," *Cell*, vol. 116, no. 2, pp. 235–246, Jan. 2004.

[3] K. Fischer, P. Cramer, R. Busch, S. Stilgenbauer, J. Bahlo, C. D. Schweighofer, S. Böttcher, P. Staib, M. Kiehl, M. J. Eckart, G. Kranz, V. Goede, T. Elter, A. Bühler, D. Winkler, M. Kneba, H. Döhner, B. F. Eichhorst, M. Hallek, and C.-M. Wendtner, "Bendamustine combined with rituximab in patients with relapsed and/or refractory chronic lymphocytic leukemia: a multicenter phase II trial of the German Chronic Lymphocytic Leukemia Study Group," *J. Clin. Oncol.*, vol. 29, no. 26, pp. 3559–66, Sep. 2011.

[4] B. Turgut, O. Vural, F. S. Pala, G. E. Pamuk, K. Tabakcioglu, M. Demir, S. Ongören, T. Soysal, and C. Algünes, "17p deletion is associated with resistance of B-cell chron-

ic lymphocytic leukemia cells to in vitro fludarabine-induced apoptosis.," *Leuk. Lymphoma*, vol. 48, pp. 311–20, 2007.

[5] L. R. Martins, P. Lúcio, A. Melão, I. Antunes, B. A. Cardoso, R. Stansfield, M. T. S. Bertilaccio, P. Ghia, D. Drygin, M. G. Silva, and J. T. Barata, "Activity of the clinical-stage CK2-specific inhibitor CX-4945 against chronic lymphocytic leukemia," *Leukemia*, vol. 28, no. 1, pp. 179–82, Jan. 2014.

[6] E. Y. O. and S. A. R. Marina A. Orlova, "Effect of 67Zn-nanoparticles on leukemic cells and normal lymphocytes," *Br. J. Med. Med. Res.*, vol. 2, pp. 21–30, 2012.

[7] D. Trachootham, H. Zhang, W. Zhang, L. Feng, M. Du, Y. Zhou, Z. Chen, H. Pelicano, W. Plunkett, W. G. Wierda, M. J. Keating, and P. Huang, "Effective elimination of fludarabine-resistant CLL cells by PEITC through a redox-mediated mechanism," *Blood*, vol. 112, no. 5, pp. 1912–22, Sep. 2008.

[8] M. R. Grever, D. M. Lucas, G. W. Dewald, D. S. Neuberg, J. C. Reed, S. Kitada, I. W. Flinn, M. S. Tallman, F. R. Appelbaum, R. a Larson, E. Paietta, D. F. Jelinek, J. G. Gribben, and J. C. Byrd, "Comprehensive assessment of genetic and molecular features predicting outcome in patients with chronic lymphocytic leukemia: results from the US Intergroup Phase III Trial E2997," *J. Clin. Oncol.*, vol. 25, no. 7, pp. 799–804, Mar. 2007.

[9] S. a Parikh, K. G. Rabe, N. E. Kay, T. G. Call, W. Ding, S. M. Schwager, D. a Bowen, M. Conte, D. F. Jelinek, S. L. Slager, and T. D. Shanafelt, "Chronic lymphocytic leukemia in young (≤55 years) patients: a comprehensive analysis of prognostic factors and outcomes," *Haematologica*, vol. 99, no. 1, pp. 140–7, Jan. 2014.

[10] T. S. Lin, M. Moran, M. Lucas, S. Waymer, S. Jefferson, D. B. Fischer, M. R. Grever, and J. C. Byrd, "Antibody therapy for chronic lymphocytic leukemia: a promising new modality," *Hematol. Oncol. Clin. North Am.*, vol. 18, no. 4, pp. 895–913, ix–x, Aug. 2004.

[11] M. Hirose, E. Hosoi, S. Humano, and A. Jalili, "Multidrug resistance in hematological malignancy," *J. Med. Invest.*, vol. 50, no. 3–4, pp. 126–35, 2003.

[12] V. Jonsson, C. Gemmell, and A. Wiik, "Emerging concepts in the management of the malignant haematological disorders," *Expert. Opin. Pharmacother.*, vol. 1, no. 4, pp. 713–735, 2000.

[13] P. Piccaluga, G. Martinelli, and M. Baccarani, "Advances in the treatment for haematological malignancies," *Expert. Opin. Pharmacother.*, vol. 7, no. 6, pp. 721–732, 2006.

[14] M. A. Albrecht, C. W. Evans, and C. L. Raston, "Green chemistry and the health implications of nanoparticles," *Green Chem.*, vol. 8, no. 5, p. 417, May 2006.

[15] H. Hahn, "Unique features and properties of nanostructured materials," *Adv. Eng. Mater.*, vol. 5, no. 5, pp. 277–284, May 2003.

[16] A. Henglein, "Small-particle research: physicochemical properties of extremely small colloidal metal and semiconductor particles," *Chem. Rev.*, vol. 89, no. 8, pp. 1861–1873, Dec. 1989.

[17] K. Cho, X. Wang, S. Nie, Z. G. Chen, and D. M. Shin, "Therapeutic nanoparticles for drug delivery in cancer," *Clin. Cancer Res.*, vol. 14, no. 5, pp. 1310–6, Mar. 2008.

[18] M. Ferrari, "Cancer nanotechnology: opportunities and challenges," *Nat. Rev. Cancer*, vol. 5, no. 3, pp. 161–71, Mar. 2005.

[19] J. M. Koziara, P. R. Lockman, D. D. Allen, and R. J. Mumper, "In situ blood–brain barrier transport of nanoparticles," *Pharm. Res.*, vol. 20, no. 11, pp. 1772–8, Nov. 2003.

[20] M.-D. Cheng, "Effects of nanophase materials (< or = 20 nm) on biological responses," *J. Environ. Sci. Health. A. Tox. Hazard. Subst. Environ. Eng.*, vol. 39, no. 10, pp. 2691–705, Jan. 2004.

[21] K. Bogunia-Kubik and M. Sugisaka, "From molecular biology to nanotechnology and nanomedicine," *Biosystems.*, vol. 65, no. 2–3, pp. 123–38.

[22] S. M. Moghimi, A. C. Hunter, and J. C. Murray, "Nanomedicine: current status and future prospects," *FASEB J.*, vol. 19, no. 3, pp. 311–30, Mar. 2005.

[23] W. E. Bawarski, E. Chidlowsky, D. J. Bharali, and S. a Mousa, "Emerging nanopharmaceuticals," *Nanomedicine*, vol. 4, no. 4, pp. 273–82, Dec. 2008.

[24] N. Ashammakhi, "Nanosize, mega-impact, potential for medical applications of nanotechnology," *J. Craniofac. Surg.*, vol. 17, no. 1, pp. 3–7, Jan. 2006.

[25] S. Auvinen, M. Alatalo, H. Haario, J.-P. Jalava, and R.-J. Lamminmaki, "Size and Shape Dependence of the Electronic and Spectral Properties in TiO 2 Nanoparticles," *J. Phys. Chem. C*, vol. 115, no. 17, pp. 8484–8493, May 2011.

[26] X. He, W. Zhong, C.-T. Au, and Y. Du, "Size dependence of the magnetic properties of Ni nanoparticles prepared by thermal decomposition method," *Nanoscale Res. Lett.*, vol. 8, no. 1, p. 446, Jan. 2013.

[27] O. Aktsipetrov, P. Elyutin, A. Nikulin, and E. Ostrovskaya, "Size effects in optical second-harmonic generation by metallic nanocrystals and semiconductor quantum dots: the role of quantum chaotic dynamics," *Phys. Rev. B. Condens. Matter*, vol. 51, no. 24, pp. 17591–17599, Jun. 1995.

[28] R. Bakalova, H. Ohba, Z. Zhelev, M. Ishikawa, and Y. Baba, "Quantum dots as photosensitizers?," *Nat. Biotechnol.*, vol. 22, no. 11, pp. 1360–1, Nov. 2004.

[29] H. Zhang, B. Chen, and J. F. Banfield, "Particle Size and pH Effects on Nanoparticle Dissolution," *J. Phys. Chem. C*, vol. 114, no. 35, pp. 14876–14884, Sep. 2010.

[30] A. M. Schrand, M. F. Rahman, S. M. Hussain, J. J. Schlager, D. A. Smith, and A. F. Syed, "Metal-based nanoparticles and their toxicity assessment," *Wiley Interdiscip. Rev. Nanomed. Nanobiotechnol.*, vol. 2, no. 5, pp. 544–68.

[31] A. Nel, T. Xia, L. Mädler, and N. Li, "Toxic potential of materials at the nanolevel," *Science*, vol. 311, no. 5761, pp. 622–7, Feb. 2006.

[32] S. Nair, A. Sasidharan, V. V Divya Rani, D. Menon, S. Nair, K. Manzoor, and S. Raina, "Role of size scale of ZnO nanoparticles and microparticles on toxicity toward bacteria and osteoblast cancer cells," *J. Mater. Sci. Mater. Med.*, vol. 20 Suppl 1, pp. S235–41, Dec. 2009.

[33] A. C. S. Samia, X. Chen, and C. Burda, "Semiconductor quantum dots for photodynamic therapy," *J. Am. Chem. Soc.*, vol. 125, no. 51, pp. 15736–7, Dec. 2003.

[34] I. L. Medintz, H. T. Uyeda, E. R. Goldman, and H. Mattoussi, "Quantum dot bioconjugates for imaging, labelling and sensing," *Nat. Mater.*, vol. 4, no. 6, pp. 435–46, Jun. 2005.

[35] A. A. B. Vladimir A Fonoberov, "ZnO quantum dots: physical properties and optoelectronic applications," *J. Nanoelectron. Optoelectron.*, vol. 1, 2006.

[36] K. M. Reddy, K. Feris, J. Bell, D. G. Wingett, C. Hanley, and A. Punnoose, "Selective toxicity of zinc oxide nanoparticles to prokaryotic and eukaryotic systems," *Appl. Phys. Lett.*, vol. 90, no. 213902. pp. 2139021–2139023, 24-May-2007.

[37] G. Oberdörster, E. Oberdörster, and J. Oberdörster, "Nanotoxicology: an emerging discipline evolving from studies of ultrafine particles," *Environ. Health Perspect.*, vol. 113, no. 7, pp. 823–39, Jul. 2005.

[38] N. C. Mueller and B. Nowack, "Exposure modeling of engineered nanoparticles in the environment," *Environ. Sci. Technol.*, vol. 42, no. 12, pp. 4447–4453, Jun. 2008.

[39] S. Singh and H. S. Nalwa, "Nanotechnology and health safety—toxicity and risk assessments of nanostructured materials on human health," *J. Nanosci. Nanotechnol.*, vol. 7, no. 9, pp. 3048–70, Sep. 2007.

[40] C. Sinico and A. Fadda, "Vesicular carriers for dermal drug delivery," *Expert. Opin. Drug Deliv.*, vol. 6, no. 8, pp. 813–825, 2009.

[41] T. Islam and L. Josephson, "Current state and future applications of active targeting in malignancies using superparamagnetic iron oxide nanoparticles," *Cancer Biomark.*, vol. 5, no. 2, pp. 99–107, 2009.

[42] D. Rao, M. Forrest, A. Alani, G. Kwon, and J. Robinson, "Biodegradable PLGA based nanoparticles for sustained regional lymphatic drug delivery," *J. Pharm. Sci.*, vol. 99, no. 4, pp. 2018–31, 2010.

[43] L. Guopei, Y. Xianjun, J. Chen, Y. Feng, F. Deliang, and L. Weiyue, "LyP-1-conjugated nanoparticles for targeting drug delivery to lymphatic metastatic tumors," *Int. J. Pharm.*, vol. 385, no. 1–2, pp. 150–156, 2010.

[44] J. Arias, L. Reddy, and P. Couvreur, "Polymeric nanoparticulate system augmented the anticancer therapeutic efficacy of gemcitabine," *J. Drug Target.*, vol. 17, no. 8, pp. 586–98, 2009.

[45] Y. Matsumura, "Polymeric micellar delivery systems in oncology," *Jpn. J. Clin. Oncol.*, vol. 38, no. 12, pp. 793–802, 2008.

[46] J. Enbäck and P. Laakkonen, "Tumour-homing peptides—tools for targeting, imaging and destruction," *Biochem. Soc. Trans.*, vol. 35, no. Pt 4, pp. 780–3, 2007.

[47] E. Mansilla, G. H. Marin, L. Nuñez, H. Drago, F. Sturla, C. Mertz, L. Rivera, T. Ichim, N. Riordan, and C. Raimondi, "The lysosomotropic agent, hydroxychloroquine, delivered in a biodegradable nanoparticle system, overcomes drug resistance of B-chronic lymphocytic leukemia cells in vitro," *Cancer Biother. Radiopharm.*, vol. 25, no. 1, pp. 97–103, Feb. 2010.

[48] D. K. Chatterjee, L. S. Fong, and Y. Zhang, "Nanoparticles in photodynamic therapy: an emerging paradigm," *Adv. Drug Deliv. Rev.*, vol. 60, no. 15, pp. 1627–37, Dec. 2008.

[49] E. Ricci-Júnior and J. M. Marchetti, "Zinc(II) phthalocyanine loaded PLGA nanoparticles for photodynamic therapy use," *Int. J. Pharm.*, vol. 310, no. 1–2, pp. 187–95, Mar. 2006.

[50] E. Mansilla, G. Marin, and L. Núñez, "Present and future application of nanoparticle based therapies in B-chronic lymphocytic leukemia (B-CLL)," in *intechopen.com*, no. 3, 2012, pp. 431–448.

[51] S. Ostrovsky, G. Kazimirsky, A. Gedanken, and C. Brodie, "Selective cytotoxic effect of ZnO nanoparticles on glioma cells," *Nano Res.*, vol. 2, no. 11, pp. 882–890, Nov. 2009.

[52] Y.-N. Wu, D.-H. Chen, X.-Y. Shi, C.-C. Lian, T.-Y. Wang, C.-S. Yeh, K. R. Ratinac, P. Thordarson, F. Braet, and D.-B. Shieh, "Cancer-cell-specific cytotoxicity of non-oxidized iron elements in iron core-gold shell NPs," *Nanomedicine*, vol. 7, no. 4, pp. 420–7, Aug. 2011.

[53] R. Ullah and J. Dutta, "Photocatalytic degradation of organic dyes with manganese-doped ZnO nanoparticles," *J. Hazard. Mater.*, vol. 156, no. 1–3, pp. 194–200, Aug. 2008.

[54] L. Jing, K. Ding, S. Kalytchuk, Y. Wang, R. Qiao, S. V. Kershaw, A. L. Rogach, and M. Gao, "Aqueous manganese-doped core/shell CdTe/ZnS quantum dots with strong fluorescence and high relaxivity," *J. Phys. Chem. C*, vol. 117, no. 36, pp. 18752–18761, Sep. 2013.

[55] R. Bhargava, D. Gallagher, X. Hong, and A. Nurmikko, "Optical properties of manganese-doped nanocrystals of ZnS," *Phys. Rev. Lett.*, vol. 72, no. 3, pp. 416–419, Jan. 1994.

[56] P. T. Schumacker, "Reactive oxygen species in cancer cells: live by the sword, die by the sword," *Cancer Cell*, vol. 10, no. 3, pp. 175–6, Sep. 2006.

[57] J. C. Byrd, T. S. Lin, and M. R. Grever, "Treatment of relapsed chronic lymphocytic leukemia: old and new therapies," *Seminars in oncology*, vol. 33, no. 2. pp. 210–9, Apr-2006.

[58] M. J. Akhtar, M. Ahamed, S. Kumar, M. M. Khan, J. Ahmad, and S. a Alrokayan, "Zinc oxide nanoparticles selectively induce apoptosis in human cancer cells through reactive oxygen species," *Int. J. Nanomedicine*, vol. 7, pp. 845–57, Jan. 2012.

[59] C. Hanley, J. Layne, A. Punnoose, K. M. Reddy, I. Coombs, A. Coombs, K. Feris, and D. Wingett, "Preferential killing of cancer cells and activated human T cells using ZnO nanoparticles," *Nanotechnology*, vol. 19, no. 29. p. 295103, 23-Jul-2008.

[60] D. Bechet, P. Couleaud, C. Frochot, M.-L. Viriot, F. Guillemin, and M. Barberi-Heyob, "Nanoparticles as vehicles for delivery of photodynamic therapy agents," *Trends Biotechnol.*, vol. 26, no. 11, pp. 612–21, Dec. 2008.

[61] P. Juzenas, R. Generalov, N. Generalova, and I. Christensen, "Quantum dots and nanoparticles for photodynamic and radiation therapies of cancer," *Adv. Drug Deliv. Rev.*, vol. 60, no. 15, pp. 1600–14, 2008.

[62] Z. L. Wang, X. Y. Kong, Y. Ding, P. Gao, W. L. Hughes, R. Yang, and Y. Zhang, "Semiconducting and Piezoelectric Oxide Nanostructures Induced by Polar Surfaces," *Adv. Funct. Mater.*, vol. 14, no. 10, pp. 943–956, Oct. 2004.

[63] J. Zhou, N. S. Xu, and Z. L. Wang, "Dissolving behavior and stability of ZnO wires in biofluids: a study on biodegradability and biocompatibility of ZnO nanostructures," *Adv. Mater.*, vol. 18, no. 18, pp. 2432–2435, Sep. 2006.

[64] "Chemical and thermal stability of the characteristics of filtered vacuum arc deposited ZnO, SnO2 and zinc stannate thin films—abstract," *J. Phys. D. Appl. Phys.*, vol. 40, no. 17, pp. 1088–99, 2007.

[65] U. Ozgur, Y. I. Alivov, C. Liu, A. Teke, M. A. Reshchikov, S. Dogan, V. Avrutin, S.-J. Cho, and H. Morkoc, "A comprehensive review of ZnO materials and devices," *J. Appl. Phys.*, vol. 98, no. 4, p. 041301, Aug. 2005.

[66] A. H. Mokdad, J. S. Marks, D. F. Stroup, and J. L. Gerberding, "Actual causes of death in the United States, 2000," *JAMA*, vol. 291, no. 10, pp. 1238–45, Mar. 2004.

[67] G. Danaei, S. Vander Hoorn, A. D. Lopez, C. J. L. Murray, and M. Ezzati, "Causes of cancer in the world: comparative risk assessment of nine behavioural and environmental risk factors," *Lancet*, vol. 366, no. 9499, pp. 1784–93, Nov. 2005.

[68] Z. Huang, "A review of progress in clinical photodynamic therapy," *Technol. Cancer Res. Treat.*, vol. 4, no. 3, pp. 283–93, Jun. 2005.

[69] M. E. B. Tamesis and J. G. Morelli, "Vitiligo treatment in childhood: a state of the art review," *Pediatr. Dermatol.*, vol. 27, no. 5, pp. 437–45.

[70] J. N. Silva, P. Filipe, P. Morlière, J.-C. Mazière, J. P. Freitas, J. L. Cirne de Castro, and R. Santus, "Photodynamic therapies: principles and present medical applications," *Biomed. Mater. Eng.*, vol. 16, no. 4 Suppl, pp. S147–54, Jan. 2006.

[71] W. W. Yu, E. Chang, R. Drezek, and V. L. Colvin, "Water-soluble quantum dots for biomedical applications," *Biochem. Biophys. Res. Commun.*, vol. 348, no. 3, pp. 781–6, Sep. 2006.

[72] F. Wilkinson, W. Helman, and A. Ross, "Quantum yields for the photosensitized formation of the lowest electronically excited singlet state of molecular oxygen in solution," *J. Phys.*, pp. 1–29, 1993.

[73] R. C. DeRosa, M, "Photosensitized singlet oxygen and its applications," *Coord. Chem. Rev.*, vol. 233–234, no. null, pp. 351–371, Nov. 2002.

[74] J. P. Tardivo, A. Del Giglio, C. S. de Oliveira, D. S. Gabrielli, H. C. Junqueira, D. B. Tada, D. Severino, R. de Fátima Turchiello, and M. S. Baptista, "Methylene blue in photodynamic therapy: from basic mechanisms to clinical applications," *Photodiagnosis Photodyn. Ther.*, vol. 2, no. 3, pp. 175–191, Sep. 2005.

[75] D. Tada, L. Vono, E. Duarte, and R. Itri, "Methylene blue-containing silica-coated magnetic particles: a potential magnetic carrier for photodynamic therapy," *Langmuir*, no. 21, pp. 8194–8199, 2007.

[76] K. Takahashi, A. Yoshikawa, and A. Sandu, *Wide Bandgap Semiconductors: Fundamental Properties and Modern Photonic and Electronic Devices*. 2007, p. 357.

[77] L. Pugazhenthy, *Zinc Handbook: Properties, Processing, and Use in Design*. 1991, p. 619.

[78] X. Wang, J. Song, C. J. Summers, J. H. Ryou, P. Li, R. D. Dupuis, and Z. L. Wang, "Density-controlled growth of aligned ZnO nanowires sharing a common contact: a simple, low-cost, and mask-free technique for large-scale applications," *J. Phys. Chem. B*, vol. 110, no. 15, pp. 7720–4, Apr. 2006.

[79] A. Mang, K. Reimann, and S. Rübenacke, "Band gaps, crystal-field splitting, spin-orbit coupling, and exciton binding energies in ZnO under hydrostatic pressure," *Solid State Commun.*, vol. 94, no. 4, pp. 251–254, Apr. 1995.

[80] O. Dulub, U. Diebold, and G. Kresse, "Novel stabilization mechanism on polar surfaces: ZnO(0001)-Zn," *Phys. Rev. Lett.*, vol. 90, no. 1, p. 016102, Jan. 2003.

[81] H. S. Mansur, "Quantum dots and nanocomposites," *Wiley Interdiscip. Rev. Nanomed. Nanobiotechnol.*, vol. 2, no. 2, pp. 113–29.

[82] Y. R. Ryu, T. S. Lee, and H. W. White, "Properties of arsenic-doped p-type ZnO grown by hybrid beam deposition," *Appl. Phys. Lett.*, vol. 83, no. 1, p. 87, Jul. 2003.

[83] C. Ye, T. Tamagawa, and D. L. Polla, "Experimental studies on primary and secondary pyroelectric effects in Pb(ZrxTi1−x)O3, PbTiO3, and ZnO thin films," *J. Appl. Phys.*, vol. 70, no. 10, p. 5538, Nov. 1991.

[84] J. D. Albrecht, P. P. Ruden, S. Limpijumnong, W. R. L. Lambrecht, and K. F. Brennan, "High field electron transport properties of bulk ZnO," *J. Appl. Phys.*, vol. 86, no. 12, p. 6864, Dec. 1999.

[85] S. Jana, B. B. Srivastava, and N. Pradhan, "Correlation of dopant states and host bandgap in dual-doped semiconductor nanocrystals," *J. Phys. Chem. Lett.*, vol. 2, no. 14, pp. 1747–1752, Jul. 2011.

[86] B. B. Srivastava, S. Jana, N. S. Karan, S. Paria, N. R. Jana, D. D. Sarma, and N. Pradhan, "Highly luminescent Mn-doped ZnS nanocrystals: gram-scale synthesis," *J. Phys. Chem. Lett.*, vol. 1, no. 9, pp. 1454–1458, May 2010.

[87] M. W. Porambo, H. R. Howard, and A. L. Marsh, "Dopant effects on the photocatalytic activity of colloidal zinc sulfide semiconductor nanocrystals for the oxidation of 2-chlorophenol," *J. Phys. Chem. C*, vol. 114, no. 3, pp. 1580–1585, Jan. 2010.

[88] M. Geszke, M. Murias, L. Balan, G. Medjahdi, J. Korczynski, M. Moritz, J. Lulek, and R. Schneider, "Folic acid-conjugated core/shell ZnS:Mn/ZnS quantum dots as targeted probes for two photon fluorescence imaging of cancer cells," *Acta Biomater.*, vol. 7, no. 3, pp. 1327–38, Mar. 2011.

[89] T. K. Kundu, N. Karak, O. Barik, and S. Saha, "Optical properties of Zno nanoparticles prepared by chemical method using poly (VinylAlcohol) (PVA) as capping agent," *Int. J. Soft Comput. Eng.*

[90] S. Dumas, J.-C. Leprêtre, a. Lepellec, a. Darmanyan, and P. Jardon, "Reactivity of the photo excited forms of Hypericin, Hypocrellin A, Hypocrellin B and methylated Hypericin towards molecular oxygen," *J. Photochem. Photobiol. A. Chem.*, vol. 163, no. 3, pp. 297–306, May 2004.

[91] M. Kostka, P. Zimcik, M. Miletin, P. Klemera, K. Kopecky, and Z. Musil, "Comparison of aggregation properties and photodynamic activity of phthalocyanines and azaphthalocyanines," *J. Photochem. Photobiol. A. Chem.*, vol. 178, no. 1, pp. 16–25, Feb. 2006.

[92] A. G. Ali, F. B. Dejene, and H. C. Swart, "Effect of Mn doping on the structural and optical properties of sol-gel derived ZnO nanoparticles," *Cent. Eur. J. Phys.*, vol. 10, no. 2, pp. 478–484, Dec. 2011.

[93] Y. Abdollahi, A. H. Abdullah, Z. Zainal, and N. A. Yusof, "Synthesis and characterization of manganese doped ZnO nanoparticles," *Int. J. Basic Appl. Sci. IJBAS-IJENS.*, vol. 11, pp. 62–69, 2011.

[94] U. O. A. N. Ezema, F I, "Effect of concentration of Mn dopant ions on the structural and optical properties of zinc oxide crystals," *Dig. J. Nanomater. Biostruct.*, vol. 6, no. 1, pp. 271–278, 2011.

[95] S. Nagarajan and K. Arumugam Kuppusamy, "Extracellular synthesis of zinc oxide nanoparticle using seaweeds of gulf of Mannar, India," *J. Nanobiotechnology*, vol. 11, no. 1, pp. 2–11, Jan. 2013.

[96] A. Menon, N. Kalarikkal, and S. Thomas, "Studies on structural and optical properties of ZnO and Mn doped ZnO nanopowders," *Indian J. Nanosci.*, vol. 1, no. 2, pp. 16–24, 2013.

[97] Z. M. Gibbs, A. LaLonde, and G. J. Snyder, "Optical band gap and the Burstein–Moss effect in iodine doped PbTe using diffuse reflectance infrared Fourier transform spectroscopy," *New J. Phys.*, vol. 15, no. 7, p. 075020, Jul. 2013.

[98] V. Mote, J. Dargad, and B. Dole, "Effect of Mn Doping Concentration on Structural, Morphological and Optical Studies of ZnO Nano-particles," *Nanosci. Nanoeng.*, vol. 1, no. 2, pp. 116–122, 2013.

[99] P. Bihari, M. Vippola, S. Schultes, M. Praetner, A. G. Khandoga, C. a Reichel, C. Coester, T. Tuomi, M. Rehberg, and F. Krombach, "Optimized dispersion of nanoparticles for biological in vitro and in vivo studies," *Part. Fibre Toxicol.*, vol. 5, p. 14, Jan. 2008.

[100] S. H. Lila A Alkhtaby, "Structural and optical properties of Mn doped ZnO nanoparticles," *Asian J. Chem.*, vol. 23, no. 12, pp. 5605–5607, 2011.

[101] K. Donaldson, "Resolving the nanoparticles paradox," *Nanomedicine (Lond).*, vol. 1, no. 2, pp. 229–34, Aug. 2006.

[102] R. T. M. Boudreau, D. M. Conrad, and D. W. Hoskin, "Differential involvement of reactive oxygen species in apoptosis caused by the inhibition of protein phosphatase 2A in Jurkat and CCRF-CEM human T-leukemia cells," *Exp. Mol. Pathol.*, vol. 83, no. 3, pp. 347–56, Dec. 2007.

[103] H. Pelicano, L. Feng, Y. Zhou, J. S. Carew, E. O. Hileman, W. Plunkett, M. J. Keating, and P. Huang, "Inhibition of mitochondrial respiration: a novel strategy to enhance drug-induced apoptosis in human leukemia cells by a reactive oxygen species-mediated mechanism," *J. Biol. Chem.*, vol. 278, no. 39, pp. 37832–9, Sep. 2003.

[104] A. Manke, L. Wang, and Y. Rojanasakul, "Mechanisms of nanoparticle-induced oxidative stress and toxicity," *Biomed Res. Int.*, vol. 2013, p. 942916, Jan. 2013.

[105] W. Lin, Y. Xu, C.-C. Huang, Y. Ma, K. B. Shannon, D.-R. Chen, and Y.-W. Huang, "Toxicity of nano- and micro-sized ZnO particles in human lung epithelial cells," *J. Nanoparticle Res.*, vol. 11, no. 1, pp. 25–39, Jun. 2008.

[106] L. S. E. Fong, D. K. Chatterjee, and Y. Zhang, "Use of upconverting nanoparticles in photodynamic therapy."

[107] A. P. Castano, P. Mroz, and M. R. Hamblin, "Photodynamic therapy and anti-tumour immunity," *Nat. Rev. Cancer*, vol. 6, no. 7, pp. 535–45, Jul. 2006.

[108] D. J. Norris, A. L. Efros, and S. C. Erwin, "Doped nanocrystals," *Science*, vol. 319, no. 5871, pp. 1776–9, Mar. 2008.

[109] D. Glick, S. Barth, and K. F. Macleod, "Autophagy: cellular and molecular mechanisms," *J. Pathol.*, vol. 221, no. 1. pp. 3–12, May-2010.

[110] Y. Chen, E. McMillan-Ward, J. Kong, S. J. Israels, and S. B. Gibson, "Oxidative stress induces autophagic cell death independent of apoptosis in transformed and cancer cells," *Cell Death Differ.*, vol. 15, no. 1, pp. 171–82, Jan. 2008.

[111] S. Hackenberg, A. Scherzed, A. Gohla, A. Technau, K. Froelich, C. Ginzkey, C. Koehler, M. Burghartz, R. Hagen, and N. Kleinsasser, "Nanoparticle-induced photocatalytic head and neck squamous cell carcinoma cell death is associated with autophagy," *Nanomedicine (Lond).*, vol. 9, no. 1, pp. 21–33, Jan. 2014.